CARDIOVASCULAR DISEASE



# SGLT2 inhibitor ameliorates endothelial dysfunction associated with the common *ALDH2* alcohol flushing variant

**Hongchao Guo[1,2,3], Xuan Yu[4], Yu Liu[1,2,3], David T. Paik[1,2,3], Johanne Marie Justesen[5], Mark Chandy[1,2,3], James W. S. Jahng[1,2,3], Tiejun Zhang[1,2,3], Weijun Wu[1,2,3], Freeborn Rwere[4], Shane Rui Zhao[1,2,3], Suman Pokhrel[6], Rabindra V. Shivnaraine[7], Souhrid Mukherjee[7], Daniel J. Simon[4], Amit Manhas[1,2,3], Angela Zhang[1,2,3], Che-Hong Chen[6], Manuel A. Rivas[5], Eric R. Gross[1,4], Daria Mochly-Rosen[6], Joseph C. Wu[1,3,8]***

**The common aldehyde dehydrogenase 2 (*ALDH2*) alcohol flushing variant known as *ALDH2*2* affects ~8% of the world's population. Even in heterozygous carriers, this missense variant leads to a severe loss of ALDH2 enzymatic activity and has been linked to an increased risk of coronary artery disease (CAD). Endothelial cell (EC) dysfunction plays a determining role in all stages of CAD pathogenesis, including early-onset CAD. However, the contribution of *ALDH2*2* to EC dysfunction and its relation to CAD are not fully understood. In a large genome-wide association study (GWAS) from Biobank Japan, *ALDH2*2* was found to be one of the strongest single-nucleotide polymorphisms associated with CAD. Clinical assessment of endothelial function showed that human participants carrying *ALDH2*2* exhibited impaired vasodilation after light alcohol drinking. Using human induced pluripotent stem cell–derived ECs (iPSC-ECs) and CRISPR-Cas9–corrected *ALDH2*2* iPSC-ECs, we modeled *ALDH2*2*-induced EC dysfunction in vitro, demonstrating an increase in oxidative stress and inflammatory markers and a decrease in nitric oxide (NO) production and tube formation capacity, which was further exacerbated by ethanol exposure. We subsequently found that sodium-glucose cotransporter 2 inhibitors (SGLT2i) such as empagliflozin mitigated *ALDH2*2*-associated EC dysfunction. Studies in *ALDH2*2* knock-in mice further demonstrated that empagliflozin attenuated *ALDH2*2*-mediated vascular dysfunction in vivo. Mechanistically, empagliflozin inhibited $Na^+/H^+$-exchanger 1 (NHE-1) and activated AKT kinase and endothelial NO synthase (eNOS) pathways to ameliorate *ALDH2*2*-induced EC dysfunction. Together, our results suggest that *ALDH2*2* induces EC dysfunction and that SGLT2i may potentially be used as a preventative measure against CAD for *ALDH2*2* carriers.**



## INTRODUCTION

Coronary artery disease (CAD) is the leading cause of global mortality, accounting for an estimated 9 million annual deaths, according to the World Health Organization (*1*). The global prevalence of CAD is rising due to an aging population and the lack of innovative strategies to effectively prevent and treat CAD (*1*). Precision medicine for CAD patients with genetic variants holds promise as a new approach toward more effective prevention and treatment by understanding their physiological mechanisms and causal relevance (*2*).

CAD is a complex disease caused by the interplay among multiple genetic and environmental factors (*3*). Hundreds of genomic loci have previously been associated with CAD by genome-wide association studies (GWAS) (*4*). A single-nucleotide polymorphism (SNP) in the aldehyde dehydrogenase 2 (*ALDH2*) gene, *ALDH2*2*, also named rs671, causes a substitution of glutamate to lysine at position 504 (E504K) that alters the access of substrates to the catalytically active site of ALDH2 compared with the normal *ALDH2*1* allele (*5*). ALDH2 is a critical enzyme in the second step of alcohol metabolism. It is vital in detoxifying toxic aldehydes such as oxidative stress–derived aldehydes and alcohol-derived acetaldehyde. *ALDH2*2* carriers have diminished ALDH2 enzymatic activity, and this deficiency is associated with a variety of neurologic, cardiovascular, and dermatologic disorders; aberrant drug metabolism; and different types of cancers (*6*). A recent meta-analysis of 12 case-control studies with 3305 cases and 5016 controls shows that *ALDH2*2* is associated with a 48% increased risk of CAD (*7*). To date, however, the underlying mechanisms for the association between *ALDH2*2* and the onset of CAD remain unclear, which creates a barrier to the prevention and treatment of *ALDH2*2*-related CAD. In addition, alcohol consumption is a well-known risk factor for CAD (*8*). Although ethanol is not a primary contributor to CAD in studies of non-Asian individuals, it may have a substantial effect on *ALDH2*2* carriers of Asian descent (*9*, *10*). Thus, it is important to determine the combined effect of *ALDH2*2* and alcohol consumption on CAD to develop preventative strategies to reduce CAD risk among *ALDH2*2* carriers.

[1]Stanford Cardiovascular Institute, Stanford University School of Medicine, Stanford, CA 94305, USA. [2]Institute for Stem Cell Biology and Regenerative Medicine, Stanford University School of Medicine, Stanford, CA 94305, USA. [3]Department of Medicine (Division of Cardiology), Stanford University School of Medicine, Stanford, CA 94305, USA. [4]Department of Anesthesiology, Perioperative and Pain Medicine, Stanford University School of Medicine, Stanford, CA 94305, USA. [5]Biomedical Data Science, Stanford University School of Medicine, Stanford, CA 94305, USA. [6]Department of Chemical and Systems Biology, Stanford University School of Medicine, Stanford, CA 94305, USA. [7]Greenstone Biosciences, 3160 Porter Drive, Palo Alto, CA 94305, USA. [8]Department of Radiology, Molecular Imaging Program at Stanford, Stanford University, Stanford, CA 94305, USA.
*Corresponding author. Email: joewu@stanford.edu

Endothelial cells (ECs), important constituents of blood vessel walls, play a critical role in maintaining cardiovascular homeostasis by regulating vascular tone and structure. EC dysfunction is implicated in a wide variety of human cardiovascular diseases (*11*). Coronary EC dysfunction occurs early in the development of CAD and can affect all phases of the disease, from initiation to atherothrombotic complication (*12*). *ALDH2*2* has been associated with EC dysfunction by increasing inflammation via nuclear factor κB (NF-κB), c-Jun, and mitogen-activated protein kinase (MAPK) pathways (*13*); decreasing nitric oxide (NO) production via the dimethylarginine dimethylaminohydrolase-1 (DDAH1) and asymmetric dimethylarginine (ADMA) pathway (*14*); and elevating oxidative damage via reactive oxygen species (ROS) and toxic aldehydes such as 4-hydroxynonenal (4-HNE) (*15*). However, the detailed mechanism underlying *ALDH2*2*-induced EC dysfunction remains unclear. Here, we focused on elucidating the molecular and cellular mechanisms underlying *ALDH2*2*-related EC dysfunction in human cells and identifying strategies to mitigate EC dysfunction in patients with this genetic variant.

## RESULTS

### *ALDH2*2* is strongly associated with CAD in East Asians

*ALDH2*2* (rs671) has been associated with an increased risk of CAD in case-control studies in East Asians (*7*). However, these studies have small sample sizes. To further understand the effect of *ALDH2*2* on CAD, we performed a more extensive GWAS analysis in 29,319 CAD cases and 183,134 controls from Biobank Japan. *ALDH2*2* and 8730 other SNPs (fig. S1A and table S1) passed the genome-wide significance threshold ($P < 5 \times 10^{-8}$). Among these SNPs, rs78069066 in the intron of MAPK-activated protein kinase 5 (*MAPKAPK5*) ($P = 1.9 \times 10^{-92}$), rs4646776 in the intron of *ALDH2* ($P = 3.7 \times 10^{-92}$), and *ALDH2*2* in exon 12 of *ALDH2* ($P = 1.1 \times 10^{-91}$) were the most substantial SNPs associated with CAD (Fig. 1A). To identify other functionally relevant variants with high linkage disequilibrium (LD) with *ALDH2*2*, we generated a regional association plot of variants located around ±50-kb region of the *ALDH2*2* variant (fig. S1B). Only one SNP, rs4646776, which was identified by our initial GWAS analysis, showed a high LD relationship with *ALDH2*2*.

Because of the association of *ALDH2*2* with many human diseases (*6*), we also conducted a phenome-wide association study (PheWAS) of *ALDH2*2* with 47 human diseases from Biobank Japan. CAD was the most significant disease associated with *ALDH2*2* ($P = 1.1 \times 10^{-91}$), followed by other conditions, including esophageal cancer ($P = 6.2 \times 10^{-25}$) (fig. S1C). Epidemiological studies have also shown that *ALDH2*2* increases the risk of esophageal cancer (*16*), which supports our results indicating an association of *ALDH2*2* with CAD as well.

### *ALDH2*2* carriers exhibit clinical EC dysfunction with alcohol consumption

Because of the pivotal role of ECs in CAD, we hypothesized that the *ALDH2*2* variant contributed to EC dysfunction and the development of CAD. To determine whether *ALDH2*2* carriers exhibited clinical EC dysfunction, we used an EndoPAT device to assess endothelial vasodilator function in a noninvasive manner. The device records endothelium-mediated changes in response to brachial artery occlusion and vasodilation and calculates a reactive hyperemia index (RHI), which measures NO-dependent changes in vascular tone and correlates with the measurement of endothelial vasodilator function in the coronary arteries (*17*, *18*). RHI value positively correlates with endothelial function, and an RHI value of <1.67 is associated with endothelial dysfunction and risk of cardiovascular disease, including CAD (*19*). EndoPAT analysis was performed on human participants carrying either *ALDH2*1* wild-type (WT) ($n = 9$) or heterozygous *ALDH2* variants (*ALDH2*1/*2*) ($n = 9$) before or immediately after a single alcoholic beverage (fig. S1, D and E). Although there was no change of heart rate before or after alcohol consumption in the WT group [before: 71 ± 4 beats per minute (bpm); after: 71 ± 3 bpm], *ALDH2*1/*2* individuals showed a significantly increased heart rate after alcohol ingestion (before: 69 ± 4 bpm; after: 86 ± 5 bpm; $P < 0.0001$) (Fig. 1B; fig. S1, D and E; and table S2), which was consistent with the results from previous studies (*20*–*22*). Whereas there was an increase in RHI after one drink in the WT group (before: 1.73 ± 0.15; after: 1.97 ± 0.13; $P = 0.01$), the *ALDH2*1/*2* group showed the opposite trend in RHIs (before: 1.79 ± 0.16; after: 1.48 ± 0.19; $P = 0.02$) (Fig. 1C; fig. S1, D and E; and table S2). The average RHI value was below 1.67 in the *ALDH2*1/*2* group after one drink, indicating that *ALDH2*2* carriers exhibited acute EC dysfunction after one standard alcoholic beverage.

A recent study in Asians showed that *ALDH2*2* increased the risk of atrial fibrillation in habitual drinkers, suggesting that there may be synergistic effects of *ALDH2*2* and chronic alcohol consumption on cardiac arrhythmias (*10*). To investigate whether *ALDH2*2* was associated with higher risk of CAD in chronic drinkers, we examined genetic information and drinking status of human participants from the UK Biobank (*23*). The data were analyzed for the combinatorial effects of alcohol consumption and *ALDH2*2* on CAD. Among the 424,507 participants in the UK Biobank who currently consume alcohol, 73,423 were defined as chronic drinkers by the self-reported criterion that they "drink more nowadays compared to 10 years ago." Using logistic regression analysis, we found that chronic alcohol consumption in *ALDH2*2* carriers led to an approximately fourfold greater risk for CAD than their WT *ALDH2*1* counterparts, suggesting that chronic alcohol consumption increases the rate of CAD among *ALDH2*2* carriers (fig. S1F). Thus, these data suggest that *ALDH2*2* variant carriers who consume alcohol are more susceptible to EC dysfunction and CAD.

### iPSC-ECs with *ALDH2*2* show impaired EC function

To uncover the precise genotype-phenotype relationship, we used induced pluripotent stem cell (iPSC)–derived ECs (iPSC-ECs) to model *ALDH2**2-associated EC dysfunction in vitro. We recruited a cohort of 10 age- and sex-matched East Asian individuals who carried either the WT or *ALDH2*1/*2* allele as previously described ($n = 5$ per group; fig. S2A) (*24*). The *ALDH2* genotype was confirmed with Sanger sequencing (fig. S2B). After a chemically defined and small molecule–based generation of endothelial differentiation protocol (fig. S2C) (*25*), iPSCs were differentiated into iPSC-ECs as a monolayer. Immunostaining assays and fluorescence-activated cell sorting (FACS) showed that both WT and *ALDH2*1/*2* iPSC-ECs expressed the endothelial marker CD31 with high purity (Fig. 2, A and B). To examine whether *ALDH2*2*-associated EC dysfunction is associated with the differential expression of *ALDH2*, we performed a Western blot on the 10 WT and *ALDH2*1/*2* iPSC-EC lines. We observed a decrease

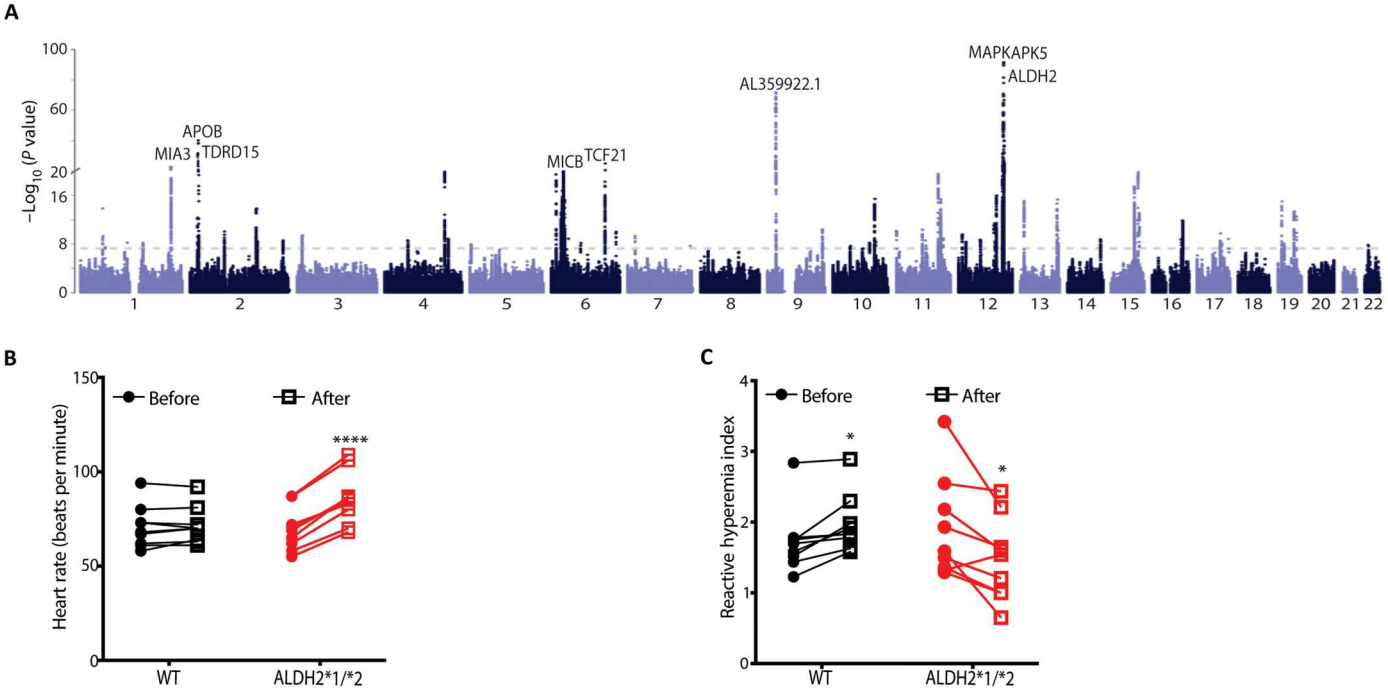


**Fig. 1. *ALDH2*2* is strongly associated with coronary artery disease (CAD) and induces endothelial dysfunction.** (**A**) Manhattan plot of GWAS on CAD using the Biobank Japan cohort. CAD cases, $n = 29{,}319$; healthy control, $n = 183{,}134$. The different colors of each block are used to distinguish data from each chromosome. The $x$ axis indicates each chromosome number (all autosomal), and the $y$ axis shows the $-\log_{10}$ ($P$ value) of risk loci. The dotted line defines the significance threshold of $P = 5 \times 10^{-8}$. The strongest genetic loci associated with CAD are labeled in the plot. (**B** and **C**) Line plots show the individual changes of heart rate (B) and reactive hyperemia index (C) before and after drinking alcohol in human participants with WT (black color) or *ALDH2*1/*2* (red color) alleles. All data are represented as means ± SEM; $n = 9$ (WT) and $n = 9$ (*ALDH2*1/*2*); "after" data compared with the "before" data, $^*P < 0.05$ and $^{****}P < 0.0001$. Statistical analyses for (B) and (C) were performed using a paired Student's $t$ test.

in ALDH2 protein in *ALDH2*1/*2* iPSC-ECs compared with WT iPSC-ECs (Fig. 2, C and D), consistent with previous studies showing a reduction in ALDH2 protein expression in the livers of human participants carrying *ALDH2*2* and in *Aldh2*$^{E487K}$ knock-in mice (*26*, *27*). As expected, ALDH2 enzymatic activity was also reduced in *ALDH2*1/*2* cell lysates relative to WT and human umbilical vein EC (HUVEC) controls (Fig. 2E).

We next measured the amount of toxic aldehyde 4-HNE in iPSC-ECs because enhanced production of toxic aldehydes such as 4-HNE has been shown to increase inflammation, oxidative stress, and cell death in patients with acute CAD (*28*, *29*). We found increased 4-HNE ($P = 0.04$) in *ALDH2*1/*2* cell lysates compared with WT controls (Fig. 2, F and G). We therefore evaluated the functional characteristics of iPSC-ECs from both WT and *ALDH2*1/*2* carriers. Compared with WT, *ALDH2*1/*2* iPSC-ECs had increased cellular ROS (Fig. 2H and fig. S2D) and a decreased capacity to generate NO (Fig. 2I and fig. S2E), which are implicated in vascular dysfunction (*30*, *31*). In addition, *ALDH2*1/*2* iPSC-ECs had increased monocyte adhesion compared with WT iPSC-ECs, suggesting increased endothelial inflammation in the *ALDH2*2* variant (Fig. 2, J and K). *ALDH2*1/*2* iPSC-ECs also showed a decreased capacity to form tubular networks versus WT iPSC-ECs (fig. S2, F and G). Thus, our data suggest a causal effect of *ALDH2*2* on EC dysfunction.

## Ethanol exacerbates *ALDH2*2*-induced EC dysfunction

Because ALDH2 is the major enzyme for metabolizing acetaldehyde from ethanol, we hypothesized that *ALDH2**2 carriers were more susceptible to the deleterious effect of ethanol on EC function. First, we determined that there were no differences in the mRNA expression of alcohol-metabolizing enzymes alcohol dehydrogenase 5 (ADH5) and ALDH2 in WT and *ALDH2*1/*2* iPSC-ECs (fig. S3A). The similar expression pattern of *ALDH2* mRNA in WT and *ALDH2*1/*2* iPSC-ECs suggested a posttranscriptional regulation of ALDH2 protein. We then treated WT and *ALDH2*1/*2* iPSC-ECs with 5 mM ethanol, the concentration of ethanol in human blood after one standard alcoholic beverage (*32*). Consistent with previous findings showing that *ALDH2*2* alone impairs endothelial function, ethanol further increased the generation of ROS (Fig. 3A), decreased NO production (Fig. 3B), increased monocyte adhesion (Fig. 3, C and D), and impaired tube formation compared with both WT (vehicle- and ethanol-treated) and vehicle-treated *ALDH2*2* iPSC-ECs (Fig. 3, E and F). These results suggest that ethanol exacerbates *ALDH2*2*-induced EC dysfunction.

## CRISPR-Cas9–corrected iPSC-ECs reverse *ALDH2*2*-induced EC dysfunction

To confirm the role of *ALDH2*2* in EC dysfunction, we next corrected *ALDH2*2* in three *ALDH2*1/*2* iPSC lines using CRISPR-Cas9 and compared EC function in three sets of WT cell lines, *ALDH2*1/*2*-corrected isogenic lines (Iso_GG), and their uncorrected counterparts. The missense *ALDH2* variant (GA) in

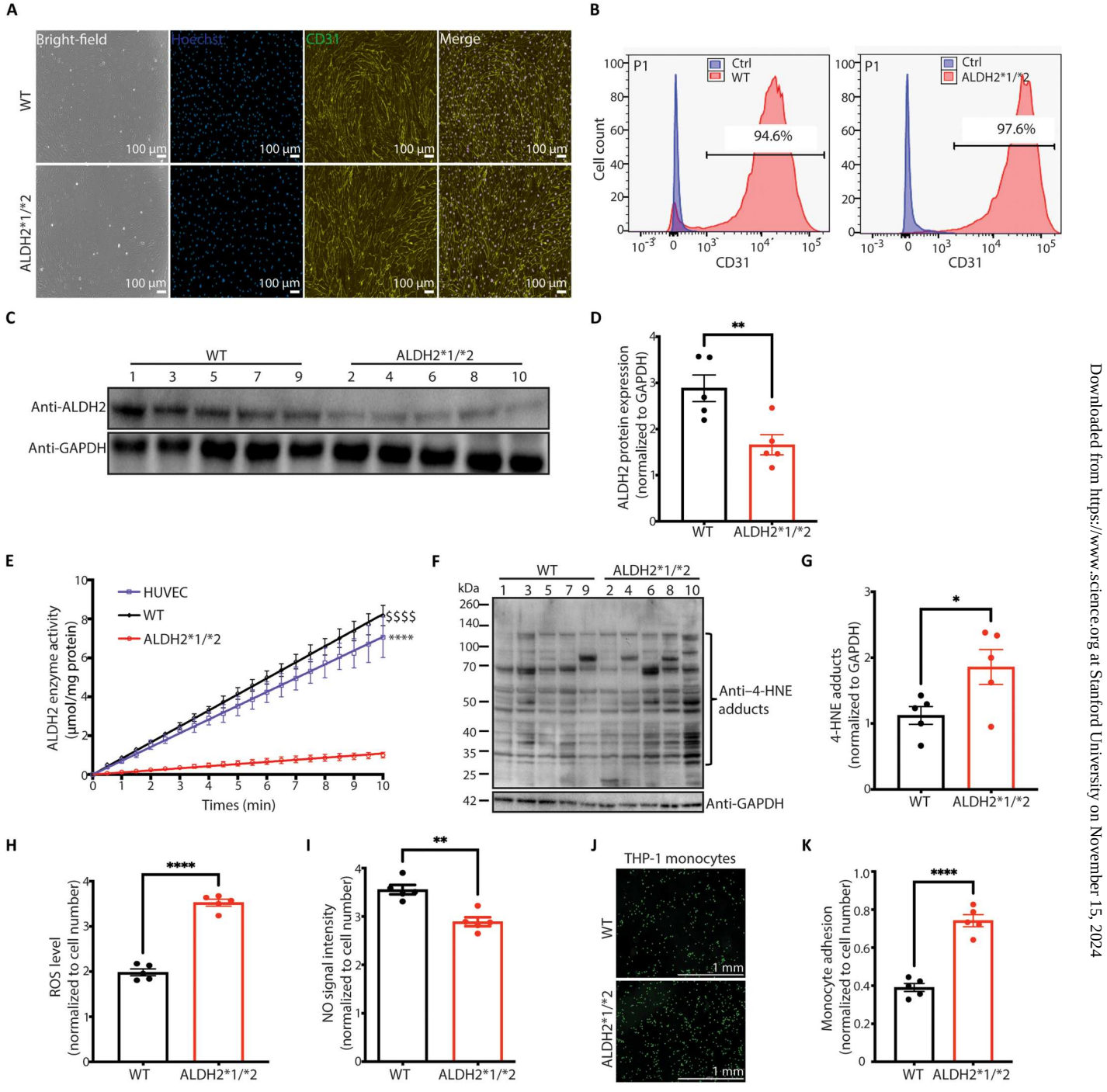


**Fig. 2. *ALDH2*2* iPSC-ECs show increased oxidative stress and monocyte adhesion and decreased NO production at baseline.** (**A**) Representative bright-field and immunofluorescence images of WT and *ALDH2*1/*2* iPSC-ECs for endothelial marker CD31 (green). Scale bars, 100 μm. (**B**) Representative fluorescence-activated cell sorting (FACS) analysis of WT and *ALDH2*1/*2* iPSC-ECs at passage 1 with CD31 antibody. (**C**) Representative immunoblot for ALDH2 in WT and *ALDH2*1/*2* iPSC-ECs. Glyceraldehyde phosphate dehydrogenase (GAPDH) was used as loading control. (**D**) Bar graph shows quantification of ALDH2 protein by immunoblot in WT and *ALDH2*1/*2* iPSC-ECs. Data are represented as relative fold change to loading control, GAPDH. $^{**}P = 0.0098$. (**E**) Enzymatic activity of ALDH2 in lysates from WT and *ALDH2*1/*2* iPSC-ECs. HUVECs were used as a positive control. WT versus *ALDH2*1/*2*: $^{\$\$\$\$}P < 0.0001$; HUVEC versus *ALDH2*1/*2*: $^{****}P < 0.0001$. (**F**) 4-Hydroxynonenal (4-HNE) adducts in WT and *ALDH2*1/*2* iPSC-ECs were assessed by Western blot with GAPDH as loading control. (**G**) Quantification of 4-HNE Western blot analysis from two technical replicates. $^{*}P = 0.04$. (**H**) Total baseline reactive oxygen species (ROS) in WT and *ALDH2*1/*2* iPSC-ECs as measured by the fluorogenic dye CM-H2DCFDA. $^{****}P < 0.0001$. (**I**) Quantification of nitric oxide (NO) production in WT and *ALDH2*1/*2* iPSC-ECs using the fluorogenic dye DAF-FM. $^{***}P = 0.001$. (**J**) Representative images of adherent THP-1 monocytes labeled with calcein AM (green) in WT and *ALDH2*1/*2* iPSC-ECs. (**K**) Quantification of monocyte adhesion in WT and *ALDH2*1/*2* iPSC-ECs. Black bar, WT iPSC-ECs; red bar, *ALDH2*1/*2* iPSC-ECs. $^{****}P < 0.0001$. All data represent five individual iPSC lines from two technical replicates per group. Data are expressed as means ± SEM. *P* values were calculated by Student's *t* test (E, H to J, and L) or two-way ANOVA with Bonferroni correction (E).

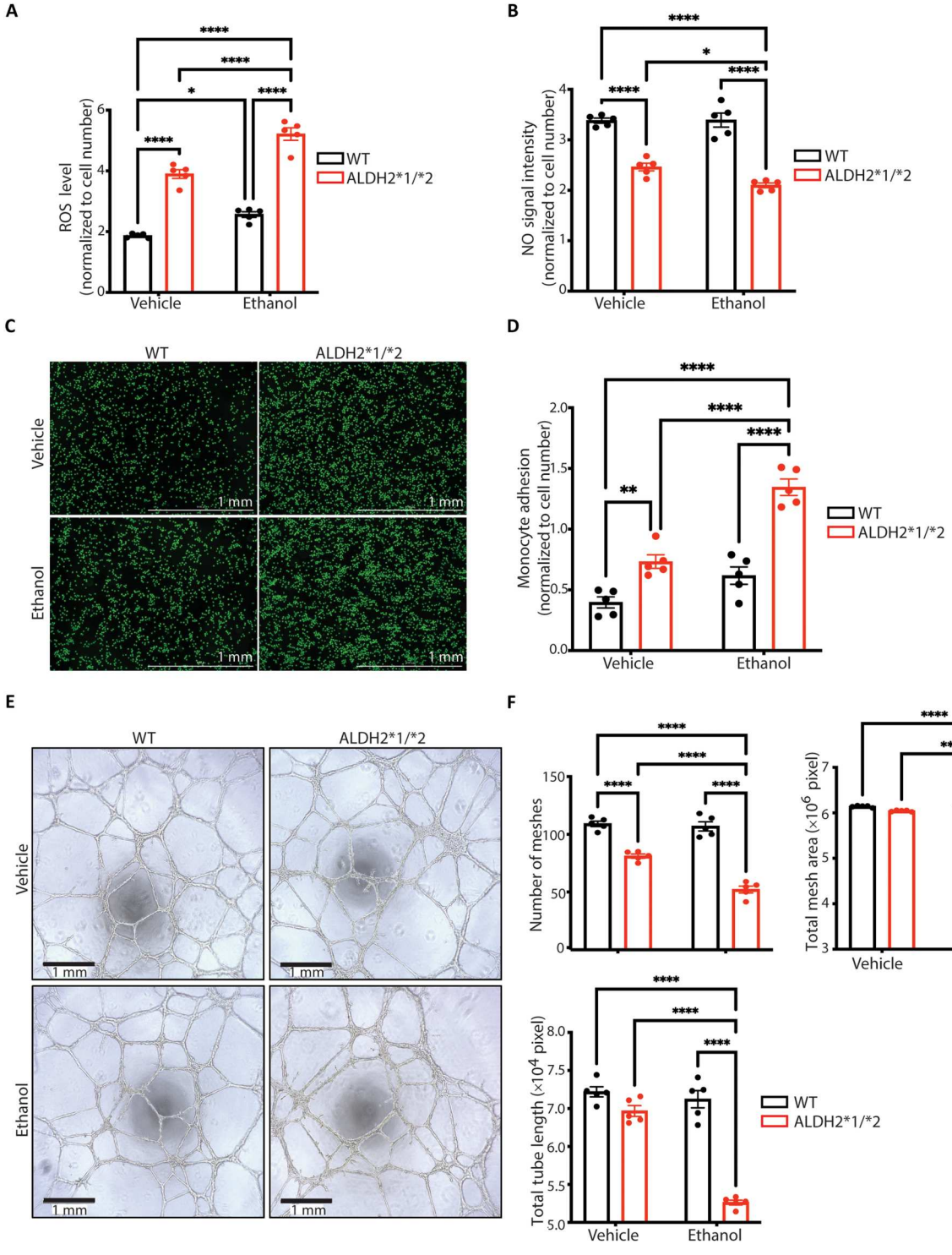


**Fig. 3. Ethanol exacerbates *ALDH2*2*-induced endothelial dysfunction.** (**A**) Measurement of cellular ROS released from WT and *ALDH2*1/*2* iPSC-ECs using the fluorogenic dye CM-H2DCFDA in the presence or absence of 5 mM ethanol. (**B**) NO production in WT and *ALDH2*1/*2* iPSC-ECs using the fluorogenic dye DAF-FM in the presence or absence of 5 mM ethanol. (**C**) Representative images of adherent THP-1 monocytes labeled with calcein AM (green) to WT and *ALDH2*1/*2* iPSC-ECs in the presence or absence of 5 mM ethanol. Scale bars, 1 mm. (**D**) Quantification of monocyte adhesion in WT and *ALDH2*1/*2* iPSC-ECs in the presence or absence of 5 mM ethanol. (**E**) Representative bright-field images of capillary-like networks formed by WT and *ALDH2*1/*2* iPSC-ECs in the presence or absence of 5 mM ethanol. Scale bars, 1 mm. (**F**) Quantitative data from the tube formation assay in WT and *ALDH2*1/*2* iPSC-ECs in the presence or absence of 5 mM ethanol. Black bar, WT iPSC-ECs; red bar, *ALDH2*1/*2* iPSC-ECs. All data represent five individual iPSC lines from two technical replicates per group. Data are expressed as means ± SEM. **P* < 0.05, ***P* < 0.01 and *****P* < 0.0001, calculated by a two-way ANOVA with Bonferroni correction.

*ALDH2*1/*2* lines was corrected and confirmed by Sanger sequencing (Fig. 4, A and B). Next, the Iso_GG iPSC lines were differentiated into ECs, and all showed high EC purity (fig. S3, B and C). As expected, ALDH2 enzyme activity was restored after gene correction (Fig. 4C). The EC dysfunction observed in *ALDH2*1/*2* iPSC-ECs was also reversed in the genome-edited Iso_GG iPSC-ECs, as evidenced by reduced ROS concentrations (Fig. 4D) and monocyte adhesion (Fig. 4, E and F) and increased NO production (Fig. 4G) and tube formation (fig. S3, D to G). Ethanol treatment did not affect *ALDH2* expression in corrected cells (fig. S3, H and I). Similarly, ethanol-induced exacerbation of EC dysfunction was also mitigated in Iso_GG iPSC-ECs (Fig. 4, G to I, and fig. S3, D to G). These findings indicate a causal role of *ALDH2*2* in EC dysfunction.

### Transcriptional profiling reveals down-regulation of the AKT/eNOS pathway in *ALDH2*2* ECs

To elucidate the molecular mechanisms of EC dysfunction, we performed bulk RNA sequencing (RNA-seq) on two *ALDH2*2*-corrected isogenic iPSC-EC lines (Iso_GG) and their uncorrected counterparts (*ALDH2*1/*2*). A direct comparison of total RNA expression between *ALDH2*1/*2* iPSC-ECs and Iso_GG controls revealed 1460 differentially expressed genes (DEGs), of which 803 were up-regulated and 657 were down-regulated (Fig. 5A and table S3). Among these DEGs, 14 were related to angiogenesis genes such as secreted frizzled-related protein 1 (*SFRP1*) and protein tyrosine kinase 2 (*PTK2*), 21 were related to antioxidants or oxidants such as glutathione *S*-transferase pi 1 (*GSTP1*) and thioredoxin reductase 2 (*TXNRD2*), and 147 were related to inflammatory genes such as interleukin-18 (*IL18*) and intercellular adhesion molecule-1 (*ICAM1*) (Fig. 5B and table S4). ICAM1 is essential in mediating monocyte adhesion to ECs (*33*). IL-18 belongs to the IL-1 family and is a prospective and independent marker of CAD risk (*34*). Quantitative polymerase chain reaction (qPCR) analysis confirmed expression of *ICAM1*, and *IL18* was up-regulated in *ALDH2*1/*2* compared with Iso_GG iPSC-ECs. In addition, ethanol further increased the expression of *ICAM1* and *IL18* in *ALDH2*1/*2* iPSC-ECs, but not in Iso_GG iPSC-ECs, suggesting that *ICAM1* and *IL18* may contribute to the inflammatory phenotype in *ALDH2*1/*2* iPSC-ECs (Fig. 5C). GSTP1 is a critical enzyme in reducing oxidative stress by increasing glutathione availability, and mutations in this gene have been associated with greater susceptibility to CAD (*35*, *36*). The expression of *GSTP1* was down-regulated in *ALDH2*1/*2* iPSC-ECs and further decreased in ethanol-treated *ALDH2*1/*2* iPSC-ECs, indicating that GSTP1 may play a role in the *ALDH2*2*-mediated increase in oxidative stress (Fig. 5C). *SFRP1*, an endogenous modulator of canonical wingless and int-1 (Wnt) signaling pathway with implications for cardiac neovascularization after injury (*37*), was also down-regulated in *ALDH2*1/*2* iPSC-ECs and further decreased in ethanol-treated *ALDH2*1/*2* iPSC-ECs (Fig. 5C), indicating that SFRP1 may be involved in *ALDH2*2*-dependent angiogenesis defects.

Gene ontology analysis of DEGs showed multiple dysregulated pathways in *ALDH2*1/*2* iPSC-ECs compared with Iso_GG iPSC-ECs (Fig. 5D). For example, genes associated with extracellular matrix (ECM)–receptor interaction, phosphoinositide 3-kinase (PI3K)–AKT signaling, relaxin signaling, MAPK signaling, and adenosine monophosphate (AMP)–activated protein kinase (AMPK) signaling pathways were down-regulated, whereas genes associated with nucleotide-binding oligomerization domain (NOD)–like receptor signaling, cellular senescence, calcium signaling, FoxO signaling, p53, and NF-κB signaling pathways were up-regulated in *ALDH2*1/*2* iPSC-ECs (Fig. 5D and table S5). AKT plays a vital role in vascular homeostasis and pathogenesis by mediating EC death, migration, and production or degradation of ECM (*38*). Our results further confirmed that the abundance of the active form of AKT, p-AKT (phosphorylation at serine-473), rather than total AKT, was decreased in *ALDH2*1/*2* iPSC-ECs (Fig. 5, E and F). The abundance of p-AKT was further reduced by ethanol treatment in *ALDH2*1/*2* iPSC-ECs, indicating that both the *ALDH2*2* variant and ethanol could limit AKT activity. Because endothelial NO synthase (eNOS) is activated by AKT-dependent phosphorylation in ECs (*39*), we used Western blot analysis to demonstrate that the active form of eNOS, p-eNOS (phosphorylation at serine-1177), was decreased in *ALDH2*1/*2* iPSC-ECs and further decreased by ethanol treatment (Fig. 5, E and F). We confirmed the relevance of this pathway by treating cells with SC79, a pan-AKT activator that specifically enhances AKT phosphorylation and activation (*40*). We found that increased AKT activity led to increased NO production and decreased ROS generation in both Iso_GG and *ALDH2*1/*2* iPSC-ECs (Fig. 5G). Thus, these findings suggest that inhibition of the AKT/eNOS pathway mediates *ALDH2*2*-induced EC dysfunction.

### SGLT2i counteracts *ALDH2*2*-associated EC dysfunction

Human iPSC-derived cells provide a unique platform to screen for compounds that have human-specific drug responsiveness (*41*). With ROS, NO, and inflammation as primary targets, we searched cardiovascular drugs approved by the U.S. Food and Drug Administration (FDA) and identified seven drugs that regulate these pathways (Fig. 6A). Three of these were sodium-glucose cotransporter 2 inhibitors (SGLT2i) (empagliflozin, canagliflozin, and dapagliflozin), which have previously been shown to induce NO production and reduce ROS generation in ECs (*42*, *43*). We used Alda-1, an activator of both WT ALDH2 and ALDH2*2 (*44*), as a positive control. Our analysis revealed that all SGLT2i showed a dose-dependent decrease in ROS generation and increase in NO production in *ALDH2*1/*2* iPSC-ECs (Fig. 6, B and C). Aspirin and metformin promoted NO generation, but they also increased ROS production. Meanwhile, fenofibrate and Alda-1 required a large dose to effectively reduce ROS. Alda-1 did not have a beneficial effect in Iso_GG iPSC-ECs, which was likely due to the high dose of Alda-1, as shown by a decrease of NO in Iso_GG iPSC-ECs (Fig. 6, B and C). Empagliflozin was selected for use in all subsequent experiments because it was efficacious for increasing NO production and reducing ROS generation at the lowest dose. A dose of 5 μM empagliflozin was selected on the basis of the cellular experiments for rescuing capacity. We then treated iPSC-ECs with 5 μM empagliflozin in the presence of ethanol (5 mM) and found that empagliflozin not only decreased ROS (fig. S4A) and increased NO production (fig. S4B) but also reduced monocyte adhesion (fig. S4, C and D) and increased EC tube formation in *ALDH2*1/*2* samples (fig. S4, E and F). Empagliflozin also reduced monocyte adhesion in Iso_GG iPSC-ECs (fig. S4, C and D), indicating that empagliflozin may reduce the proinflammatory phenotype even in the absence of the *ALDH2*2* variant. Together, these results suggested that empagliflozin improves EC dysfunction in *ALDH2*1/*2* iPSC-ECs.

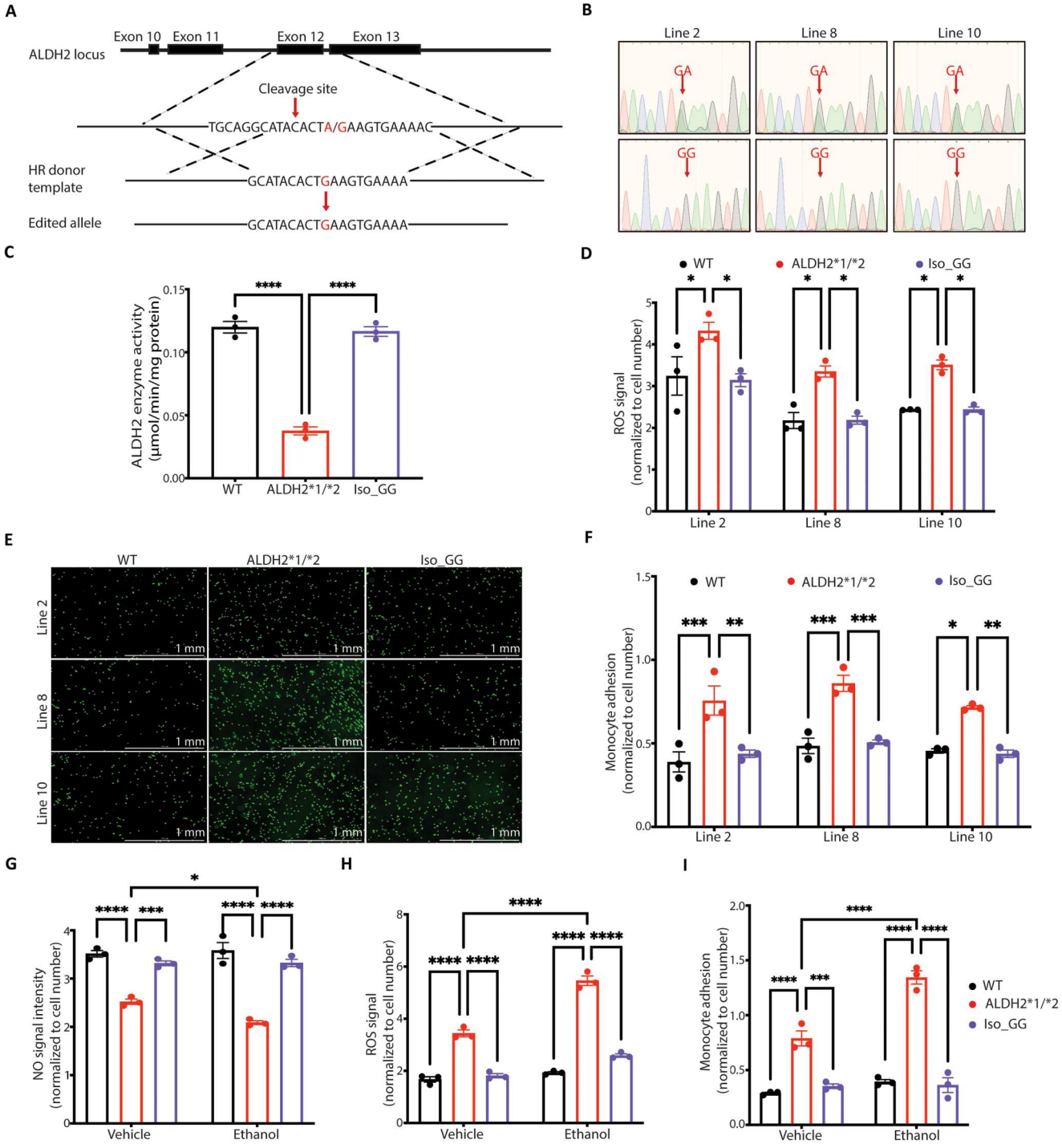


**Fig. 4. Genome-corrected isogenic *ALDH2* iPSC-ECs rescue EC dysfunction phenotype.** (**A**) CRISPR-Cas9–mediated genome modification to correct heterozygous *ALDH2*1/*2* variant (GA) into isogenic WT (Iso_GG) iPSCs using homologous repair (HR). CRISPR-Cas9 was designed to specifically cleave near the nucleotide position 111803962 at exon 12 of the *ALDH2* locus. The *ALDH2*1/*2* allele (GA) is shown in red. (**B**) Sequencing chromatogram showing three Iso_GG iPSC lines generated from their respective *ALDH2*1/*2* (GA) iPSC lines. The risk allele A is substituted by G after genome editing, as shown at the bottom (indicated by red arrows). (**C**) Enzymatic activity of ALDH2 in lysates from WT, *ALDH2*1/*2*, and Iso_GG iPSC-ECs. (**D**) Cellular ROS in WT, *ALDH2*1/*2*, and Iso_GG iPSC-ECs. Cellular ROS was quantified using CM-H2DCFDA dye. (**E**) Representative images of adherent THP-1 monocytes (green) to WT, *ALDH2*1/*2*, and Iso_GG iPSC-ECs. Scale bars, 1 mm. (**F**) Quantification of monocyte adhesion in WT, *ALDH2*1/*2*, and Iso_GG iPSC-ECs. (**G**) NO production was determined in WT, *ALDH2*1/*2*, and Iso_GG iPSC-ECs using DAF-FM in the presence or absence of 5 mM ethanol. (**H**) Measurement of ROS in WT, *ALDH2*1/*2*, and Iso_GG iPSC-ECs using CM-H2DCFDA in the presence or absence of 5 mM ethanol. (**I**) Quantification of monocyte adhesion in WT, *ALDH2*1/*2*, and Iso_GG iPSC-ECs in the presence or absence of 5 mM ethanol. Black bar, WT iPSC-ECs; red bar, *ALDH2*1/*2* iPSC-ECs; violet bar, Iso_GG iPSC-ECs. Data in (C) to (I) represent two technical replicates from three individual iPSC lines. All data are expressed as means ± SEM. **P* < 0.05, ***P* < 0.01, ****P* < 0.001, and *****P* < 0.0001, calculated by a one-way (C, D, and F) or two-way ANOVA (G to I) with Bonferroni correction.

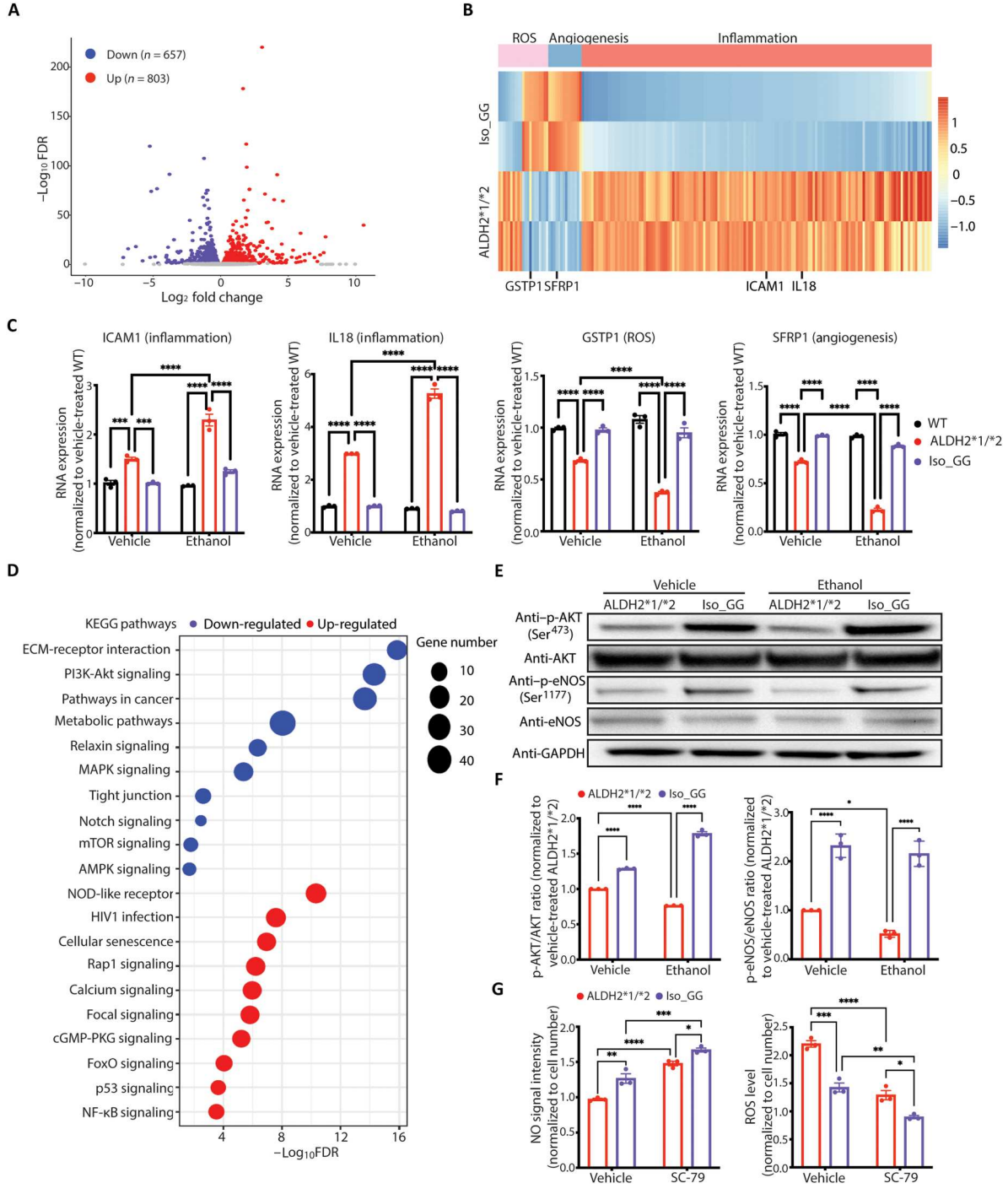


**Fig. 5. Transcriptional profiling of *ALDH2* iPSC-ECs implicates AKT/eNOS pathway in EC dysfunction.** (**A**) Volcano plot of differentially expressed genes (DEGs) between *ALDH2*1/*2* and Iso_GG iPSC-ECs. Up-regulated genes are highlighted in red, and down-regulated genes are shown in blue. False discovery rate (FDR) < 0.05 was set as a threshold of significance. (**B**) Heatmap of DEGs in oxidative stress, angiogenesis, and inflammatory pathways. Expression of representative genes is indicated on the bottom of the heatmap. *SFRP1*, secreted frizzled-related protein 1; *GSTP1*, glutathione *S*-transferase pi 1; *IL18*, interleukin-18; *ICAM1*, intercellular adhesion molecule-1. (**C**) qPCR data from *ALDH2*1/*2* and Iso_GG iPSC-ECs in the presence or absence of 5 mM ethanol. (**D**) Top 10 up-regulated (red) or down-regulated pathways (blue) in *ALDH2*1/*2* iPSC-ECs compared with Iso_GG iPSC-ECs as determined by $-\log_{10}$ FDR using the Kyoto Encyclopedia of Genes and Genomes (KEGG) pathway database. (**E**) Immunoblots for p-AKT ($Ser^{473}$), total AKT, p-eNOS ($Ser^{1177}$), and total eNOS proteins in *ALDH2*1/*2* and Iso_GG iPSC-ECs in the presence or absence of 5 mM ethanol. GAPDH was used as the loading control. (**F**) Bar graph shows quantification of p-AKT/AKT ratio and p-eNOS/eNOS ratio in WT and *ALDH2*1/*2* iPSC-ECs in the presence or absence of 5 mM ethanol. (**G**) Measurement of NO and ROS in ethanol-treated WT and *ALDH2*1/*2* iPSC-ECs in the presence or absence of the AKT activator SC79 (4 μg/ml). Vehicle, equal volume of EC medium. Black bar, WT iPSC-ECs; red bar, *ALDH2*1/*2* iPSC-ECs; violet bar, Iso_GG iPSC-ECs. Data in (C), (F), and (G) represent two independent technical replicates from three individual iPSC lines. All data are expressed as means ± SEM. **P* < 0.05, ***P* < 0.01, ****P* < 0.001, and *****P* < 0.0001, calculated by a two-way ANOVA with Bonferroni correction.

A

| Drugs | Reduce inflammation | Reduce ROS | Increase NO | Note |
|---|---|---|---|---|
| Aspirin | √ | √ | √ | Inflammatory conditions |
| Empagliflozin | √ | √ | √ | Type 2 diabetes, heart failure |
| Canaglifozin | √ | √ | √ | Type 2 diabetes, heart failure |
| Dapagliflozin | √ | √ | √ | Type 2 diabetes, heart failure |
| Atorvastatin | √ | √ | √ | Lowering LDL levels |
| Fenofibrate | √ | √ | √ | Hyper -cholesterolemia |
| Metformin | √ | √ | √ | Type 2 diabetes |
| Alda-1 | √ | √ | √ | ALDH2 activator |

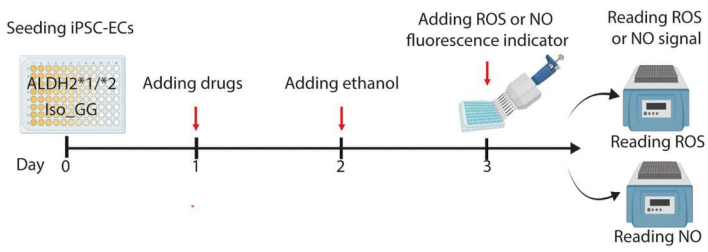


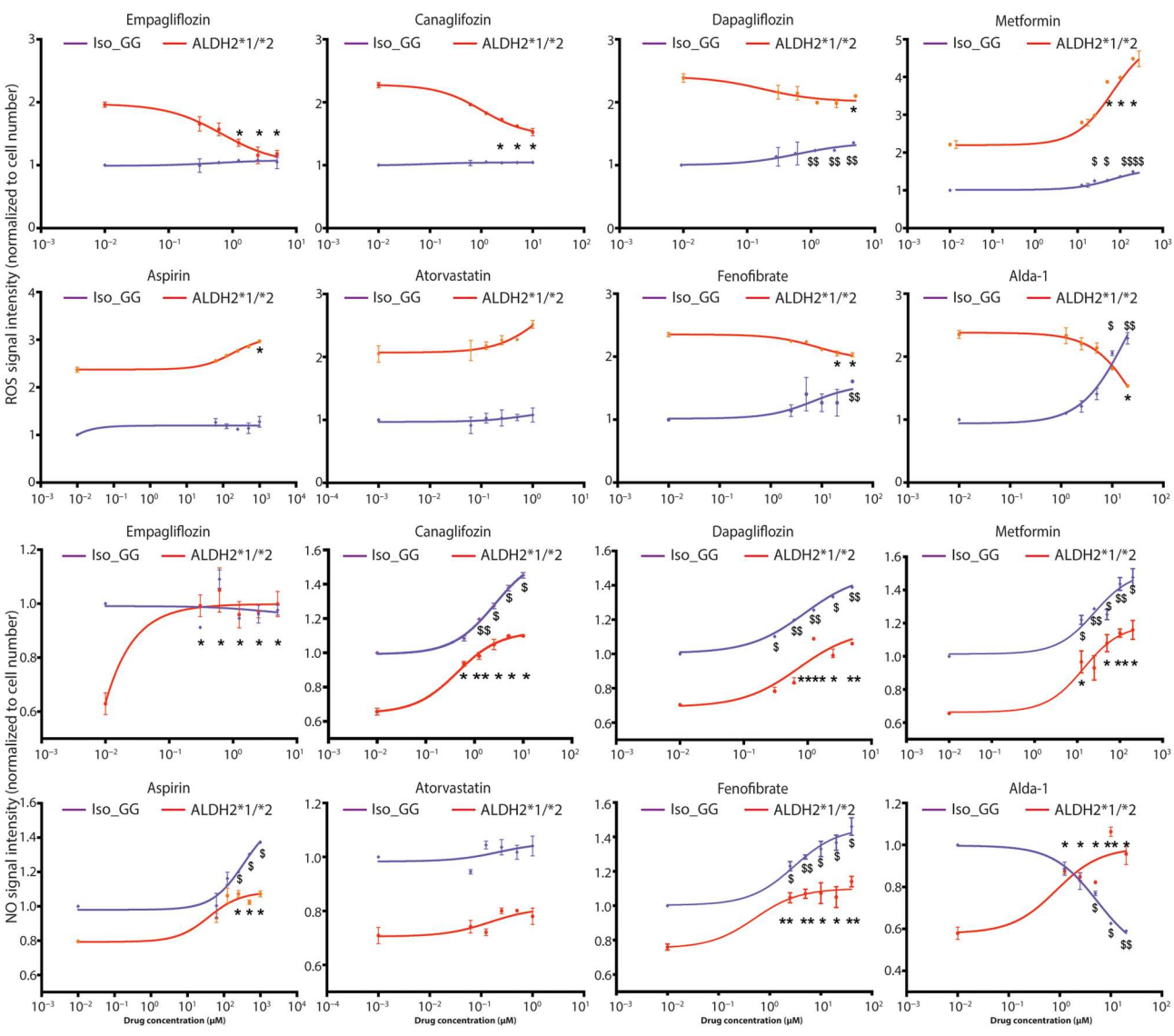


**Fig. 6. Drug screening for treatment of *ALDH2*2*-induced oxidative stress and NO impairment using iPSC-ECs.** (**A**) Table listing the eight compounds assessed and their current uses, including known effects on inflammation, ROS, and NO (left). These included seven medications approved by the FDA and the ALDH2 activator Alda-1. Schematic workflow of the experimental design (right). These drugs were assessed for their impact on ROS and NO production in Iso_GG and *ALDH2*1/*2* iPSC-ECs. iPSC-ECs were treated on day 1. Ethanol (5 mM) was added the following day, and then NO and ROS signals were measured on day 3. (**B** and **C**) Dose-response curves based on ROS generation, indicated by CM-H2DCFDA (B), and NO production indicated by DAF-FM (C) in WT and *ALDH2*1/*2* iPSC-ECs with drug treatment. Six different dosages were used for each drug, including a vehicle control (DMSO). Because of a wide range of drug dosages used in WT and *ALDH2*2* iPSC-ECs, the power of 10 format was used on the *x* axis to plot the drug response. A value of 0.01 μM ($10^{-2}$ μM) instead of 0 μM was used to indicate response to vehicle control (DMSO), and the concentrations of NO or ROS in Iso_GG or *ALDH2*1/*2* iPSC-ECs were normalized to vehicle (DMSO) treatment. Data in (B) and (C) represent three individual iPSC lines from two technical replicates for each group. Data are expressed as means ± SEM. A nonlinear regression model was applied to plot drug dose-response. Iso_GG iPSC-ECs with drug treatment compared with Iso_GG with vehicle (DMSO) treatment: $^{\$}P < 0.05$, $^{\$\$}P < 0.01$, and $^{\$\$\$\$}P < 0.0001$. *ALDH2*1/*2* iPSC-ECs with drug treatment compared with *ALDH2*1/*2* with vehicle (DMSO) treatment: $^{*}P < 0.05$, $^{**}P < 0.01$, and $^{****}P < 0.0001$, calculated by Student's *t* test.

### Empagliflozin rescues endothelial dysfunction in *ALDH2**2 mice

Next, we examined whether empagliflozin rescued endothelial dysfunction in mice in which a single human variant, E504K, was knocked into one copy of WT mouse *Aldh2* allele (heterozygous *ALDH2*1/*2*) (*26*). The *ALDH2*1/*2* mice were divided into three experimental groups: *ALDH2*1/*2* mice with the daily saline intraperitoneal injection (vehicle group), *ALDH2*1/*2* mice challenged with the daily ethanol intraperitoneal injection (20%, 1 g/kg per day) combined with osmotic pump providing polyethylene glycol (PEG) in 50% dimethyl sulfoxide (DMSO) (EtOH group), and *ALDH2*1/*2* mice with the daily ethanol intraperitoneal injection combined with osmotic pump delivering empagliflozin (10 mg/kg per day) (Empa group) (Fig. 7A). After daily saline or ethanol intraperitoneal injection for 21 days, aortas were isolated from the three groups and from saline-injected WT mice (WT group) to examine their vascular structure and function. First, we examined the structure and function of isolated aortas from untreated WT and *ALDH2*1/*2* mice using Masson's trichrome staining. The results showed no differences in aorta area and wall thickness between WT and *ALDH2*1/*2* mice (Fig. 7, B to D). We next investigated whether *ALDH2*1/*2* mice had differences in aortic contraction and relaxation compared with WT mice using a wire myograph (fig. S5A). The aortic rings isolated from the *ALDH2*1/*2* mice demonstrated a lower basal endothelial-dependent relaxation response to acetylcholine and a lower basal contractile response to endothelin-1 (ET-1) compared with the aortic rings isolated from the WT mice (fig. S5, B and C). The maximal endothelial-dependent relaxation induced by acetylcholine was 91.8 ± 1.4% in the WT group and 81.1 ± 4.0% in the *ALDH2*1/*2* group. The maximal contraction induced by ET-1 was 0.44 ± 0.03 mN/mg in the WT group and 0.35 ± 0.01 mN/mg in the *ALDH2*1/*2* group (fig. S5, B and C). These data showed that the *ALDH2*1/*2* mice have a reduced response to endothelial-dependent relaxation and contraction at baseline.

We next examined whether ethanol could induce further endothelial-dependent vascular dysfunction in the *ALDH2*1/*2* mice (*45*). We found a 24% increase in aortic area and 83% increase in wall thickness in the EtOH group relative to aortas from the vehicle group. In contrast, aortas from mice with sustained empagliflozin administration, in addition to ethanol treatment, limited vascular remodeling and reduced aorta area and wall thickness (Fig. 7, B to D). Aortic rings from the EtOH group exhibited a 42% decrease in acetylcholine-induced endothelial-dependent maximal relaxation and an 18% decrease in ET-1–induced endothelial-modified maximal contraction relative to the vehicle group (Fig. 7, E and F, and Table 1). Maximal relaxation induced by acetylcholine was 81.1 ± 4.0% in the vehicle group and 47.0 ± 13.2% in the EtOH group, whereas maximal contraction induced by ET-1 was 0.35 ± 0.01 mN/mg in the vehicle group and 0.29 ± 0.02 mN/mg in the EtOH group (Fig. 7, E and F, and Table 1). Sustained treatment with empagliflozin restored vascular function of the aortic rings in *ALDH2*1/*2* mice by enhancing acetylcholine-induced relaxation response (maximal relaxation: 91.2 ± 1.7%) and ET-1–induced contraction response (maximal contraction: 0.45 ± 0.04%), similar to WT mice (Fig. 7, E and F, and Table 1).

*ALDH2*2* has been associated with a higher incidence of endothelial dysfunction–related diseases and exacerbates coronary endothelial damage and function in type 1 diabetic mice (*13*, *46*, *47*). We therefore investigated the effect of empagliflozin on vascular function in *ALDH2*1/*2* mice with diabetes mellitus induced by streptozotocin (STZ) treatment (fig. S5D). Four weeks after induction of diabetes mellitus, aortas were isolated, and endothelial function was examined. Whereas the aortas from diabetic *ALDH2*1/*2* mice (STZ group) demonstrated a 16.5% increase in wall thickness relative to the vehicle group (fig. S5E), empagliflozin administration diminished the progress of vascular remodeling by reducing wall thickness by ~14.5% in comparison with the STZ group (fig. S5E). There was no difference in aortic area between STZ and vehicle groups (fig. S5F). Functional studies demonstrated that aortas isolated from the STZ group had a 29.8% decrease in acetylcholine-induced endothelial-dependent maximal relaxation relative to the vehicle group (fig. S5G). Here, empagliflozin administration (STZ + Empa group) restored acetylcholine-induced endothelial-dependent maximal relaxation and further enhanced ET-1–induced endothelial-modified contraction relative to the STZ group (fig. S5, G and H).

These data showed that, at baseline, the aortic contractile response to ET-1 and the endothelial-dependent relaxation response to acetylcholine were reduced in heterozygous *ALDH2*1/*2* mice compared with the WT mice despite having normal vascular structure. Ethanol exposure or diabetes mellitus induced further endothelial dysfunction by decreasing the vascular tone and increasing vascular wall thickness and aorta area in *ALDH2*1/*2* mice. Sustained cotreatment with empagliflozin restored vascular function and attenuated vascular remodeling in ethanol-treated or diabetic *ALDH2*1/*2* mice.

### Empagliflozin does not directly activate ALDH2 enzymatic activity

To determine whether empagliflozin improved *ALDH2*2*-related endothelial dysfunction through direct activation of ALDH2

**Table 1. Effects of empagliflozin on vascular function in *ALDH2*2* mice using wire myograph.** Data correspond to results presented in Fig. 7 (E and F). The maximal contractile force was recorded in response to 1 μM endothelin-1 (ET-1), and the relaxation maximal relaxation (%) was recorded in response to 1 mM acetylcholine in mouse aortas isolated from WT, vehicle, EtOH, and Empa groups. WT group, wild-type *Aldh2* mice; vehicle group, solvent (PEG/DMSO) control–treated *ALDH2*1/*2* mice; EtOH group, alcohol-treated *ALDH2*1/*2* mice; Empa group, ethanol- and Empa-treated *ALDH2*1/*2* mice. Data represent six mice for each group. Data are expressed as means ± SEM. Vehicle versus WT group: $^{\#}P < 0.05$; EtOH versus vehicle group: $^{\$}P < 0.05$; EtOH versus Empa group: $^{*}P < 0.05$, calculated by a one-way ANOVA with Bonferroni correction.

| | WT | Vehicle | EtOH | Empagliflozin |
|---|---|---|---|---|
| Maximal contractile force (mN/mg) | 0.44 ± 0.03 | 0.35 ± 0.01$^{\#}$ | 0.29 ± 0.02$^{\$}$ | 0.45 ± 0.04%$^{*}$ |
| Maximal relaxation (%) | 91.8 ± 1.4% | 81.1 ± 4.0%$^{\#}$ | 47.0 ± 13.2%$^{\$}$ | 91.2 ± 1.7%$^{*}$ |

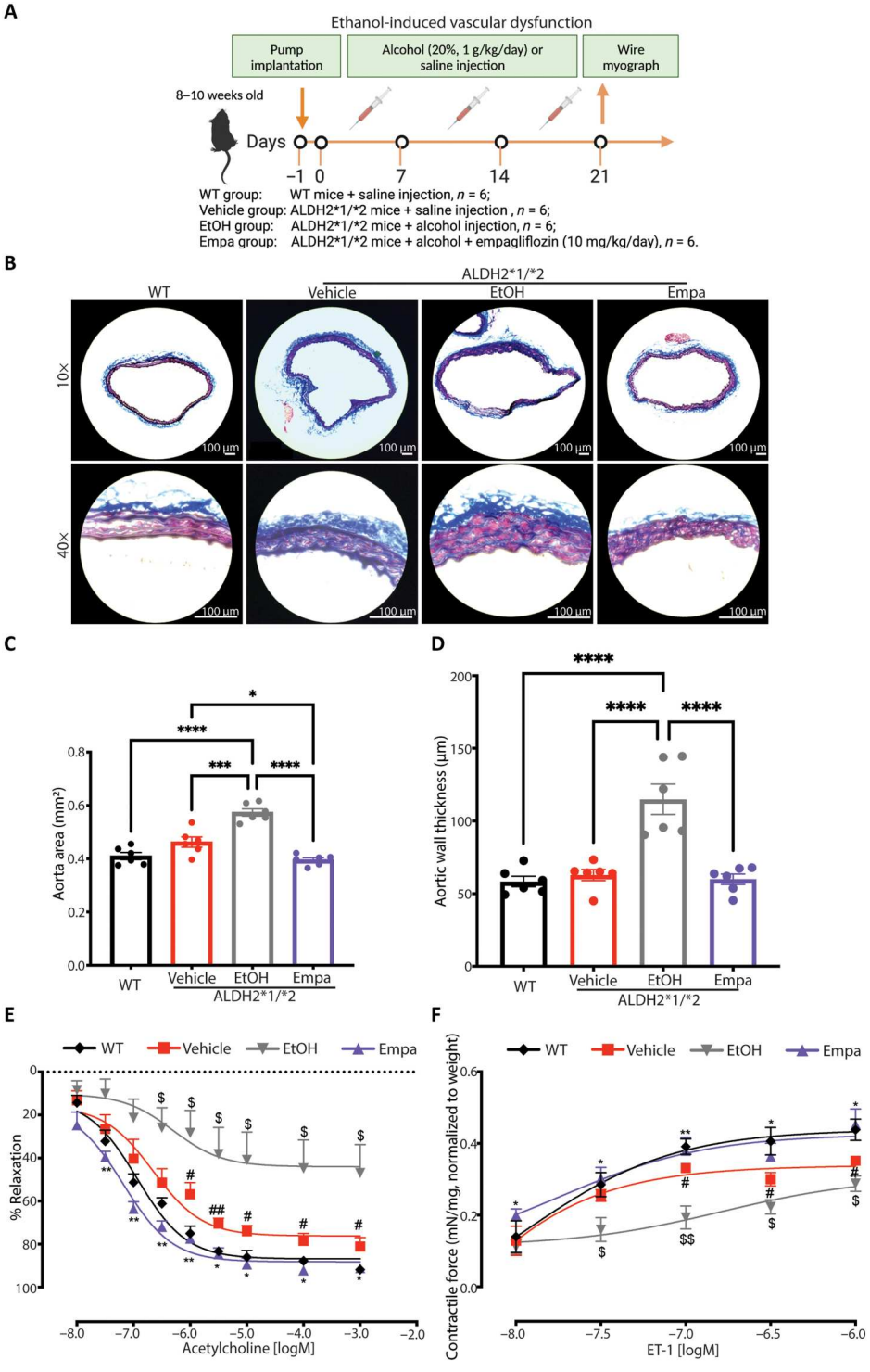


**Fig. 7. Empagliflozin alleviates vascular dysfunction in *ALDH2**1/*2* heterozygous mice.** (**A**) Schematic of the experimental design to examine the effects of empagliflozin on vascular function in ethanol-treated *ALDH2*1/*2* mice. Mice were divided into four groups: saline-injected WT mice, saline-injected *ALDH2*1/*2* (vehicle group), ethanol- and solvent (PEG/DMSO) control–treated *ALDH2*1/*2* (EtOH group), and ethanol- and Empa-treated *ALDH2*1/*2* mice (Empa group). (**B**) Representative bright-field images of Masson's trichome staining of mouse aortas from the four experimental groups above. (**C** and **D**) Quantification of aortic area and wall thickness. $^{*}P < 0.05$, $^{***}P < 0.001$, and $^{****}P < 0.0001$, calculated by a one-way ANOVA with Bonferroni correction. (**E** and **F**) Concentration-response curve for acetylcholine-induced aortic relaxation (E) and ET-1–induced aortic contraction (F) in WT, vehicle, EtOH, and Empa groups. Data represent six mice for each group. Data are expressed as means ± SEM. In (E) and (F), vehicle versus WT group: $^{\#}P < 0.05$ and $^{\#\#}P < 0.01$; EtOH versus vehicle group: $^{\$}P < 0.05$ and $P < 0.01$; EtOH versus Empa group: $^{*}P < 0.05$ and $^{**}P < 0.01$, calculated by Student's *t* test.

enzyme, we first performed induced-fit docking studies of tested drugs on ALDH2 in silico. We used the cocrystal structure of ALDH2 with a known activator, Alda-1 (Protein Data Bank ID: 3INJ), and docked empagliflozin at the same site (fig. S6, A to C) (*48*). Alda-1 was previously reported to activate the WT ALDH2 enzyme more than twofold and increase the activity of ALDH2*1/*2 to WT values (*44*). In silico analysis suggested that empagliflozin occupied the Alda-1 binding site in ALDH2 in a similar manner to Alda-1 (fig. S6, A to C), suggesting that empagliflozin may activate ALDH2 through a mechanism similar to Alda-1.

To verify these results, we assessed ALDH2 enzyme activity in vitro in the presence of empagliflozin or Alda-1 using recombinant ALDH2 protein isolated from bacteria containing one copy of the *ALDH2*1/*2* variant and one copy of the WT variant (*ALDH2*1/*2*) or two copies of the WT variant (WT). ALDH2*1/*2 enzyme activity exhibited approximately 45% of WT activity in the absence of activators, with ~1.04 μmol/min per mg of enzyme activity for ALDH2*1/*2 versus ~2.30 μmol/min per mg for WT. Empagliflozin did not enhance the activity of either WT ($P = 0.94$) or ALDH2*1/*2 ($P = 0.99$) (fig. S6D). These results suggest that empagliflozin is not a direct ALDH2 activator in vitro.

We have previously shown that Alda-1 can inhibit 4-HNE–induced ALDH2 inactivation (*44*). We therefore examined whether empagliflozin can also limit 4-HNE inactivation of ALDH2. In the presence of 50 μM 4-HNE, both WT and ALDH2*1/*2 were inactivated. As shown previously (*44*), 1 μM Alda-1 increased enzyme activity, but 5 μM empagliflozin had no effect (fig. S6E). Thus, our results indicate that empagliflozin may not directly regulate ALDH2 activity but may instead improve *ALDH2*2*-induced endothelial dysfunction indirectly.

### Empagliflozin improves *ALDH2*2*-related EC dysfunction via NHE-1/AKT/eNOS pathway

Many studies have shown that the target of empagliflozin, SGLT2, is not expressed in cardiac cells and that empagliflozin exhibits its beneficial effects on cardiovascular disease via off-target mechanisms (*49*). We also confirmed that mRNA for SGLT genes *SGLT1* and *SGLT2* was not detected in either ethanol-free or ethanol-treated Iso_GG and *ALDH2*1/*2* iPSC-ECs (fig. S7A), suggesting that the benefits of empagliflozin treatment for *ALDH2*2*-induced endothelial dysfunction may be via off-target effects. The $Na^+/H^+$ exchanger isoform-1 (*NHE-1*), sodium voltage-gated channel alpha subunit 5 (*SCN5A*), and L-type $Ca^{2+}$ channels are three targets through which empagliflozin may exert its beneficial effects on cardiovascular cells (*50*). We first examined the expression of these channels in iPSC-ECs. The $C_t$ values of *SCN5A* and L-type $Ca^{2+}$ channel genes such as calcium voltage-gated channel subunit alpha1 C (*CACAN1C*) and calcium voltage-gated channel subunit alpha1 D (*CACAN1D*) are greater than 33, indicating that the expression of *SCN5A* and L-type $Ca^{2+}$ channel genes is low in iPSC-ECs. In contrast, the $C_t$ value for *NHE1* is approximately 25, indicating higher expression (fig. S7B). Thus, we focused on the NHE-1 channel for further studies.

NHE-1 is a membrane protein that exchanges intracellular $H^+$ and extracellular $Na^+$ and plays critical roles in regulating intracellular pH and volume homeostasis. Previous studies showed that activated NHE-1 drove ROS formation in human ECs (*51*), suggesting that NHE-1 could be involved in *ALDH2*2*-related endothelial dysfunction. To test this hypothesis, we examined NHE activity ($\Delta[H^+]/s$) and cytoplasmic $Na^+$ in Iso_GG and *ALDH2*1/*2* iPSC-ECs. NHE-1 activity in *ALDH2*1/*2* iPSC-ECs was higher compared with Iso_GG iPSC-ECs (Iso_GG: −0.55 ± 0.02; *ALDH2*1/*2*: −0.66 ± 0.02) (Fig. 8A). In addition, the concentration of cytoplasmic $Na^+$ in *ALDH2*1/*2* iPSC-ECs was higher than in the Iso_GG group (Iso_GG: 0.79 ± 0.01 versus *ALDH2*1/*2*: 0.87 ± 0.002), which also indicated higher NHE-1 activity (Fig. 8B). Empagliflozin decreased $\Delta[H^+]/s$ (Empa: −0.56 ± 0.02) and cytoplasmic $Na^+$ (Empa: 0.80 ± 0.03) in *ALDH2*1/*2* iPSC-ECs, suggesting that empagliflozin may regulate endothelial NHE-1 activity (Fig. 8, A and B). Furthermore, cariporide, an NHE-1 inhibitor, was applied to iPSC-ECs in the presence or absence of empagliflozin. As expected, cariporide reduced NHE-1 activity (Car: −0.55 ± 0.02) and cytoplasmic $Na^+$ (Car: 0.78 ± 0.02) in *ALDH2*1/*2* iPSC-ECs (Fig. 8, A and B). However, there was no further reduction of NHE-1 activity in *ALDH2*1/*2* iPSC-ECs (Car + Empa: −0.54 ± 0.01) and $Na^+$ (Car + Empa: 0.76 ± 0.003) when empagliflozin and cariporide were combined, suggesting that empagliflozin directly targets NHE-1 (Fig. 8, A and B, and fig. S7, C to E).

Next, in silico induced-fit docking studies were performed, and the ability of empagliflozin to bind NHE-1 was assessed based on a comparison of the docking score and ligand stability to cariporide (*52*). The results showed that empagliflozin bound well to NHE-1 in its most stable binding pose (the docking score was −5.20 for Empa and −5.58 for Car) (Fig. 8C). However, empagliflozin had a more stable interaction compared with cariporide. The total interaction energy was −200 kJ/mol for empagliflozin and −160 kJ/mol for cariporide based on a 100-ns simulation with a 10-ps sampling rate (fig. S7, F and G, and movies S1 and S2). Thus, the data suggest that empagliflozin improves *ALDH2*2*-related EC dysfunction by targeting NHE-1.

Next, the effects of empagliflozin on ROS and NO production were examined in Iso_GG and *ALDH2*1/*2* iPSC-ECs in the presence of cariporide. Whereas cariporide increased NO production and decreased ROS generation in *ALDH2*1/*2* iPSC-ECs, there were no further changes with the addition of empagliflozin, suggesting that empagliflozin ameliorates *ALDH2*2*-related NO reduction and oxidative stress by inhibiting NHE-1 activity (Fig. 8, D and E). In addition, we determined whether empagliflozin can regulate AKT in *ALDH2*1/*2* iPSC-ECs via NHE-1. Western blot analysis showed that the total AKT protein and the active form of AKT, p-AKT, were increased in both empagliflozin- and cariporide-treated *ALDH2*1/*2* iPSC-ECs (Fig. 8, F and G). Cariporide increased AKT activity more than empagliflozin; however, there was no further improvement of AKT activity in cotreatment of cariporide and empagliflozin, suggesting that empagliflozin regulates AKT activity by inhibiting NHE-1 (Fig. 8, F and G). We also found that eNOS activity (p-eNOS/eNOS ratio) in *ALDH2*1/*2* iPSC-ECs was significantly increased with empagliflozin or cariporide treatment ($P < 0.0001$ for Empa and $P = 0.002$ for Car) (Fig. 8H). The effect of eNOS activity and NO production was stronger with empagliflozin, which may be due to additional off-target effects of empagliflozin on eNOS (*53*). These findings suggested that empagliflozin alleviates *ALDH2*2*-induced oxidative stress and NO reduction via the NHE-1/AKT/eNOS pathway.

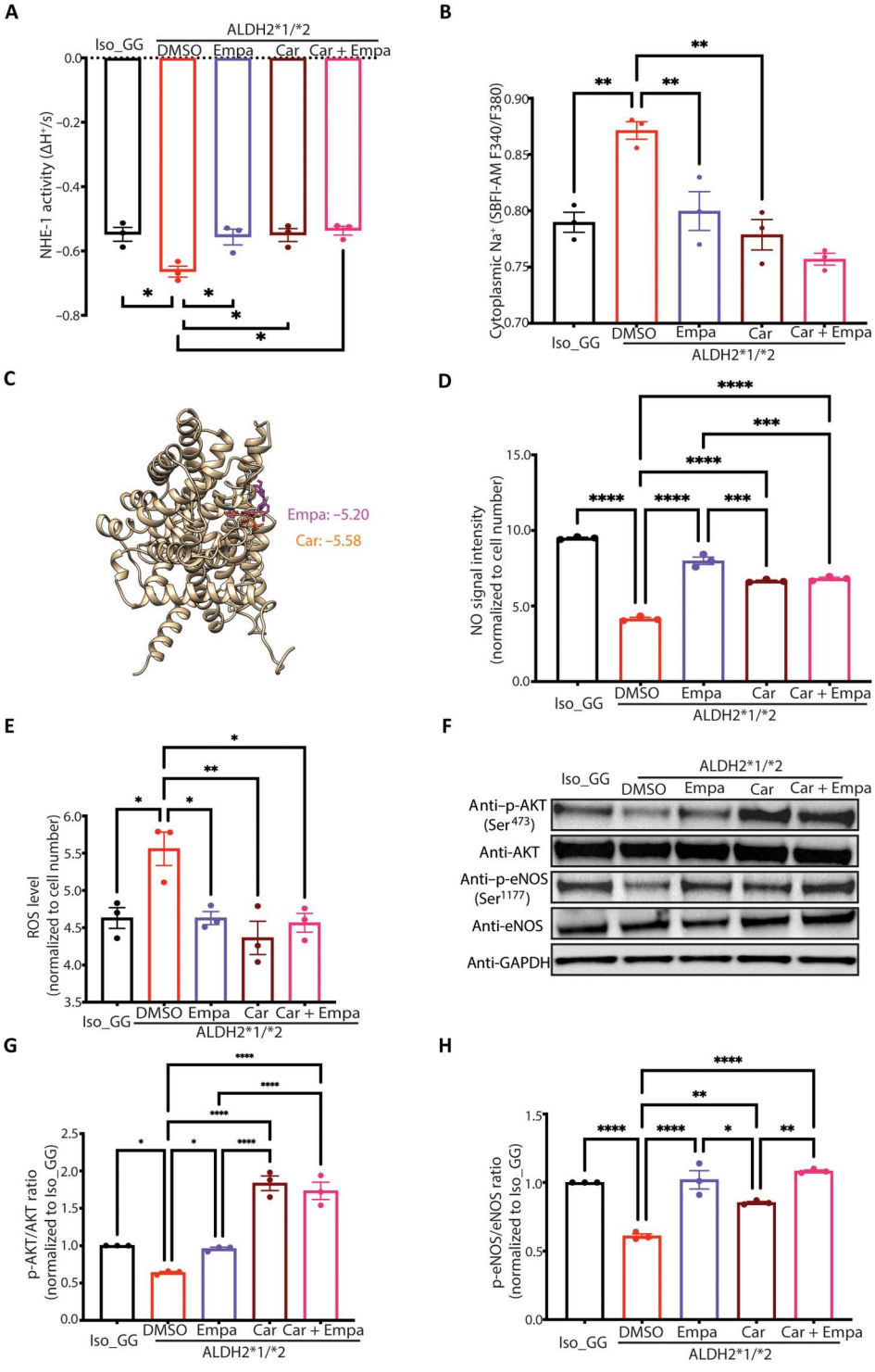


**Fig. 8. Empagliflozin improves *ALDH2*2*-related endothelial dysfunction through the NHE-1/AKT/eNOS pathway.** (**A** and **B**) Bar graphs show quantification of NHE-1 activity (A) and intracellular $Na^+$ (B) in Iso_GG and *ALDH2*1/*2* iPSC-ECs in the presence or absence of Empa (5 μM), Car (10 μM), or Car (10 μM) plus Empa (5 μM) (Car + Empa). DMSO served as vehicle. (**C**) In silico induced-fit docking showing Empa (magenta) bound to NHE-1 with a similar binding site to Car (orange). (**D** and **E**) Cellular NO (D) and ROS (E) in Iso_GG and *ALDH2*1/*2* iPSC-ECs in the presence or absence of 5 μM Empa, 10 μM Car, or Car + Empa. (**F**) Representative immunoblots show p-AKT ($Ser^{473}$), total AKT, p-eNOS ($Ser^{1177}$), and total eNOS proteins in Iso_GG and *ALDH2*1/*2* iPSC-ECs in the presence or absence of 5 μM Empa, 10 μM Car, or Car + Empa. DMSO was used as vehicle. GAPDH was used as loading control. (**G** and **H**) Bar graphs show quantification of p-AKT to total AKT ratios (G) and p-eNOS to total eNOS ratios (H) in Iso_GG and *ALDH2*1/*2* iPSC-ECs in the presence or absence of Empa (5 μM), Car (10 μM), or Car + Empa. Data represent three individual iPSC lines from two technical replicates. Data are expressed as means ± SEM. **P* < 0.05, ***P* < 0.01, ****P* < 0.001, and *****P* < 0.0001, calculated by one-way ANOVA with Bonferroni correction.

## DISCUSSION

As the most common enzymopathy caused by a single SNP in humans, the *ALDH2*2* variant has been linked to a broad spectrum of human diseases, including CAD, cancer, diabetes mellitus, and atherosclerosis (*54*). Most of these diseases are associated with vascular dysfunction (*55*). The endothelium is a delicate monolayer of cells lining all blood vessels and plays a pivotal role in the physiologic regulation of vascular tone and function (*55*). However, the role of endothelium in these diseases, especially in *ALDH2*2*-related CAD, remains unclear (*56*). In this study, we found that one standard drink of alcohol impaired endothelial vasodilator function in human participants with the *ALDH2*2* variant, but not in WT carriers. We did not observe baseline differences in EC function between WT and *ALDH2*1/*2* human participants, but this may be due to the complex mechanisms of homeostasis in the human body (*57*). Data from iPSC-ECs derived from human participants revealed EC dysfunction in *ALDH2*2* carriers by increased ROS and proinflammation and reduced NO production and tube formation, which have been linked to the onset and development of CAD (*12*). Our data also demonstrated the adverse effects of *ALDH2*2* and alcohol consumption on EC dysfunction and CAD. Given the prevalence of CAD in *ALDH2*2* carriers (*58*, *59*), identification of *ALDH2*2* in patients with CAD may be used to educate individuals and provide guidance regarding alcohol consumption.

We used transcriptome profiling to identify down-regulation of the AKT pathway in *ALDH2*2* iPSC-ECs and found that it may play a crucial role in *ALDH2*2*-related EC dysfunction. We also found that impaired ALDH2 enzyme activity in the *ALDH2*2* genotype led to elevated ROS and decreased NO through AKT and eNOS signaling, suggesting that these pathways could also be targeted for intervention (*28*). One study has demonstrated that ALDH2 rescues myocardial ischemia/reperfusion injury by activating the AKT pathway (*60*). Our data also suggested that AKT activation by SC79 may be an intervention to limit *ALDH2*2*-related CAD. However, overexpression of AKT has also been shown to have adverse effects on ECs through the development of vascular malformations (*61*). Therefore, downstream factors of AKT will need to be identified to more precisely target its pathological role in *ALDH2*2*-related CAD.

We previously found that *ALDH2*2* mice exhibited higher concentrations of proinflammatory cytokines that are further exacerbated with chronic moderate ethanol exposure of 1 g/kg per day (*62*) relative to WT mice (*63*). Here, transcriptome profiling revealed that up-regulation of AMPK, MAPK, and NF-κB signaling pathways was associated with *ALDH2*2*-related EC dysfunction. These pathways have been shown to mediate *ALDH2*-related inflammation and atherosclerotic plaque formation in mouse and cell models (*13*, *64*), suggesting that they may also be targeted to reduce or inhibit *ALDH2*2*-induced EC dysfunction.

Another strategy we explored was to directly increase the catalytic activity and stability of ALDH2*2 with small molecules. We used the small-molecule Alda-1 and showed a dose-dependent increase in NO and a decrease in ROS in *ALDH2*1/*2* iPSC-ECs. However, at a high dose, it has a toxic effect on ECs in culture. After searching for FDA-approved drugs with cardiovascular benefit, we found that SGLT2i improved endothelial dysfunction in *ALDH2*1/*2* iPSC-ECs. Recently, SGLT2i, including empagliflozin, were found to have beneficial effects for cardiovascular disease, including heart failure, myocardial infarction, and hypertension (*42*). In addition, a recent study showed the combined positive effect of Alda-1 and empagliflozin on diabetes-associated HFpEF in mice, indicating that empagliflozin could be repurposed for preventing and treating *ALDH2*2*-related CAD (*65*). However, a more comprehensive test in human participants is needed to confirm that empagliflozin prevents EC dysfunction in *ALDH2*2* carriers.

SGLT2 is mainly expressed in the kidney and has not been detected in cardiac cells (*66*). We confirmed that SGLT mRNAs were not expressed in iPSC-ECs, suggesting that empagliflozin may improve EC function independently of its action on the sodium-glucose cotransporter. Although our in silico results and those of others (*67*) showed that empagliflozin could potentially activate ALDH2 enzyme activity, our subsequent in vitro data demonstrated that empagliflozin did not directly activate ALDH2 or limit 4-HNE–induced adducts. The benefits of empagliflozin on *ALDH2*2*-related endothelial dysfunction may therefore be due to other off-target effects (*68*).

Empagliflozin has been shown to activate AMPK (*69*), promote AKT/eNOS signaling (*70*), reduce ROS generation, and restore NO bioavailability in ECs (*43*). In addition, empagliflozin was previously found to alleviate tumor necrosis factor–α (TNF-α)–mediated inflammation in ECs (*43*). However, the direct targets of these beneficial effects of empagliflozin were unknown. Here, we found that empagliflozin rescued endothelial dysfunction by inhibiting NHE-1 activity AKT/eNOS signaling. Although several functional studies have indicated that empagliflozin can directly target NHE-1, additional experiments are needed to demonstrate the physical binding of empagliflozin to NHE-1 (*71*–*74*). We also showed that the NHE-1 inhibitor cariporide could improve *ALDH2*2*-induced EC dysfunction. Earlier pilot studies have shown the beneficial effects of cariporide on cardiovascular disease, including CAD (*75*). However, cariporide failed in phase 3 clinical trials for CAD patients due to increased mortality (*75*). More recently, one study showed that cariporide could improve vascular function ex vivo in saphenous veins from *ALDH2*2* carriers (*76*), suggesting that NHE-1 may be a potential therapeutic target for follow-up studies in either specific patient populations or with other small molecules.

Our study demonstrated clinical endothelial dysfunction in healthy control participants with the *ALDH2*2* variant and moderate alcohol consumption. We further examined the mechanisms of *ALDH2*2*-mediated endothelial dysfunction and found improved *ALDH2*2*-mediated endothelial dysfunction with empagliflozin treatment in both in vitro and in vivo models. In the future, clinical trials should investigate whether the *ALDH2*2* variant and alcohol consumption exacerbate endothelial dysfunction in diabetics or those with existing CAD. These studies should also test whether empagliflozin ameliorates *ALDH2*2*-mediated atherosclerosis in the setting of diabetes or CAD. Last, another limitation of this study is that only male participants were recruited. Future studies are needed to investigate the effects of the *ALDH2*2* variant in females.

In summary, we found that even minimal alcohol consumption impaired endothelial function in human participants with the *ALDH2*2* allele. Empagliflozin ameliorated this dysfunction in vitro and in mice by inhibiting NHE-1 activity and restoring the AKT and eNOS signaling. Given the crucial role of the endothelium in vascular function, these results suggest that targeting ALDH2*2

activity and its downstream effects may be an effective strategy to limit vascular disease in *ALDH2*2* carriers (*77*).

## MATERIALS AND METHODS

### Study design

To investigate the function of the endothelium in *ALDH2*2* carriers, we recruited18 healthy volunteers carrying WT or heterozygous variant (*ALDH2*1/*2*) at Stanford University under an Institutional Review Board–approved protocol (ID: 61417). A single hair was extracted to genotype the *ALDH2* allele. The human participants were served one beer (Heineken, 12 fl oz, 5% ethanol/volume) to consume over a 30-min time period. The EndoPAT test was performed before and immediately after ethanol consumption. The sample size was determined to provide >80% power for detecting at least 20% difference of RHI between before and after ethanol consumption in *ALDH2*2* carriers at the significance of 0.05. Volunteers′ endothelial function was assessed by digital plethysmography using the EndoPAT2000 system (Itamar Medical Ltd.), and a detailed clinical history was recorded (table S2). The genotype of these human participants was not known during the test, and the results were analyzed in a blinded fashion.

To study the molecular mechanisms underlying endothelial dysfunction in the *ALDH2*2* carriers, we recruited a cohort of 10 age- and sex-matched East Asian individuals who carried either the WT or *ALDH2*1/*2* allele as previously described (table S6) (*24*). These iPSC lines were obtained from Stanford University Cardiovascular Institute Biobank and assigned to WT ($n$ = 5) or *ALDH2*1/*2* ($n$ = 5) groups based on the presence of the *ALDH2* variant. Measurements of endothelial function from both WT and individuals with the *ALDH2*2* variant were not blinded. A minimum of two technical replicates were used for each experiment.

To examine whether empagliflozin rescued endothelial dysfunction in *ALDH2* mutant mice, we tested our hypothesis using (i) *ALDH2*1/*2* knock-in mice matched to C57/BL6 WT *Aldh2* mice; (ii) ethanol-induced vascular dysfunction by injecting ethanol into the rodent peritoneum; (iii) an STZ-induced diabetic model by injecting STZ into the rodent peritoneum; and (iv) empagliflozin, an SGLT2i, delivered by osmotic pump. The knock-in *ALDH2*2* mice were generated by homologous recombination. A single-nucleotide substitution (G to A) within the *ALDH2* genomic fragment was introduced by site-directed mutagenesis corresponding to the position of human E504K mutation. The construction and phenotype of *ALDH2*1/*2* knock-in mice have been described previously (*26*). An experimental group size of six or greater animals was used to detect at least a 20% difference with a power of 95% and $P < 0.05$. All procedures in this study were performed in accordance with the animal protocols approved by the Animal Care and Use Committee of Stanford University (ID: 34047). Wire myograph tests were performed by observers blinded to the treatment groups. All animals were randomized, and the genotype test and drug treatments were blinded.

### Statistical analysis

Data were analyzed using Prism (GraphPad) or Excel and reported as means ± SEM. Comparisons were measured by one-way analysis of variance (ANOVA), two-way ANOVA test with Bonferroni correction for experiments with more than two groups, or by two-tailed Student′s $t$ test for experiments with two groups. A $P$ value of <0.05 was considered statistically significant. For GWAS in Fig. 1A and PheWAS in fig. S1, the SNP-phenotype association was analyzed using linear or logistic regression models, and age, gender, and principal components were adjusted as covariates. Further details can be found in the Supplementary Materials.

## Supplementary Materials

**This PDF file includes:**
Materials and Methods
Figs. S1 to S7
Tables S2, S6 and S7
References (*78*–*88*)

**Other Supplementary Material for this manuscript includes the following:**
Tables S1, S3 to S5
Movies S1 and S2
Data files S1 and S2
MDAR Reproducibility Checklist

View/request a protocol for this paper from *Bio-protocol*.

## REFERENCES AND NOTES


1. M. A. Khan, M. J. Hashim, H. Mustafa, M. Y. Baniyas, S. Al Suwaidi, R. AlKatheeri, F. M. K. Alblooshi, M. Almatrooshi, M. E. H. Alzaabi, R. S. Al Darmaki, S. Lootah, Global epidemiology of ischemic heart disease: Results from the Global Burden of Disease Study. *Cureus* **12**, e9349 (2020).
2. J. A. Leopold, J. Loscalzo, Emerging role of precision medicine in cardiovascular disease. *Circ. Res.* **122**, 1302–1315 (2018).
3. P. J. Talmud, Gene-environment interaction and its impact on coronary heart disease risk. *Nutr. Metab. Cardiovasc. Dis.* **17**, 148–152 (2007).
4. T. Kessler, H. Schunkert, Coronary artery disease genetics enlightened by genome-wide association studies. *JACC Basic Transl. Sci.* **6**, 610–623 (2021).
5. H. N. Larson, H. Weiner, T. D. Hurley, Disruption of the coenzyme binding site and dimer interface revealed in the crystal structure of mitochondrial aldehyde dehydrogenase "Asian" variant. *J. Biol. Chem.* **280**, 30550–30556 (2005).
6. E. R. Gross, V. O. Zambelli, B. A. Small, J. C. Ferreira, C. H. Chen, D. Mochly-Rosen, A personalized medicine approach for Asian Americans with the aldehyde dehydrogenase 2*2 variant. *Annu. Rev. Pharmacol. Toxicol.* **55**, 107–127 (2015).
7. Y. Y. Li, H. Wang, J. J. Wu, H. J. Kim, X. X. Yang, H. Y. Geng, G. Gong, ALDH2 gene G487A polymorphism and coronary artery disease: A meta-analysis including 5644 participants. *J. Cell. Mol. Med.* **22**, 1666–1674 (2018).
8. D. B. Rosoff, G. Davey Smith, N. Mehta, T. K. Clarke, F. W. Lohoff, Evaluating the relationship between alcohol consumption, tobacco use, and cardiovascular disease: A multivariable Mendelian randomization study. *PLOS Med.* **17**, e1003410 (2020).
9. C. L. Hung, S. C. Chang, S. H. Chang, P. C. Chi, Y. J. Lai, S. W. Wang, Y. J. Wu, H. I. Yeh, S. J. Lin, C. H. Chen, D. Mochly-Rosen, L. Y. Wang; MAGNET Study Investigator, Genetic polymorphisms of alcohol metabolizing enzymes and alcohol consumption are associated with asymptomatic cardiac remodeling and subclinical systolic dysfunction in large community-dwelling Asians. *Alcohol Alcohol.* **52**, 638–646 (2017).
10. C. L. Hung, K. T. Sung, S. C. Chang, Y. Y. Liu, J. Y. Kuo, W. H. Huang, C. H. Su, C. C. Liu, S. Y. Tsai, C. Y. Liu, A. S. Lee, S. H. Pan, S. W. Wang, C. J. Hou, T. C. Hung, H. I. Yeh, Variant aldehyde dehydrogenase 2 (*ALDH2*2*) as a risk factor for mechanical LA substrate formation and atrial fibrillation with modest alcohol consumption in ethnic Asians. *Biomolecules* **11**, 1559 (2021).
11. S. Xu, I. Ilyas, P. J. Little, H. Li, D. Kamato, X. Zheng, S. Luo, Z. Li, P. Liu, J. Han, I. C. Harding, E. E. Ebong, S. J. Cameron, A. G. Stewart, J. Weng, Endothelial dysfunction in atherosclerotic cardiovascular diseases and beyond: From mechanism to pharmacotherapies. *Pharmacol. Rev.* **73**, 924–967 (2021).
12. Y. Matsuzawa, A. Lerman, Endothelial dysfunction and coronary artery disease: Assessment, prognosis, and treatment. *Coron. Artery Dis.* **25**, 713–724 (2014).
13. C. Pan, J. H. Xing, C. Zhang, Y. M. Zhang, L. T. Zhang, S. J. Wei, M. X. Zhang, X. P. Wang, Q. H. Yuan, L. Xue, J. L. Wang, Z. Q. Cui, Y. Zhang, F. Xu, Y. G. Chen, Aldehyde dehydrogenase 2 inhibits inflammatory response and regulates atherosclerotic plaque. *Oncotarget* **7**, 35562–35576 (2016).

14. Y. J. Guo, L. Chen, Y. P. Bai, L. Li, J. Sun, G. G. Zhang, T. L. Yang, J. Xia, Y. J. Li, X. P. Chen, The ALDH2 Glu504Lys polymorphism is associated with coronary artery disease in Han Chinese: Relation with endothelial ADMA levels. *Atherosclerosis* **211**, 545–550 (2010).
15. G. Nannelli, E. Terzuoli, V. Giorgio, S. Donnini, P. Lupetti, A. Giachetti, P. Bernardi, M. Ziche, ALDH2 activity reduces mitochondrial oxygen reserve capacity in endothelial cells and induces senescence properties. *Oxid. Med. Cell. Longev.* , 9765027 (2018).
16. S. J. Yang, A. Yokoyama, T. Yokoyama, Y. C. Huang, S. Y. Wu, Y. Shao, J. Niu, J. Wang, Y. Liu, X. Q. Zhou, C. X. Yang, Relationship between genetic polymorphisms of ALDH2 and ADH1B and esophageal cancer risk: A meta-analysis. *World J. Gastroenterol.* **16**, 4210–4220 (2010).
17. R. Rubinshtein, J. T. Kuvin, M. Soffler, R. J. Lennon, S. Lavi, R. E. Nelson, G. M. Pumper, L. O. Lerman, A. Lerman, Assessment of endothelial function by non-invasive peripheral arterial tonometry predicts late cardiovascular adverse events. *Eur. Heart J.* **31**, 1142–1148 (2010).
18. M. M. Michelsen, N. D. Mygind, A. Pena, A. Aziz, D. Frestad, N. Host, E. Prescott; Steering Committee of the iPOWER Study, Peripheral reactive hyperemia index and coronary microvascular function in women with no obstructive CAD: The iPOWER study. *JACC Cardiovasc. Imaging* **9**, 411–417 (2016).
19. P. O. Bonetti, G. M. Pumper, S. T. Higano, D. R. Holmes, J. T. Kuvin, A. Lerman, Noninvasive identification of patients with early coronary atherosclerosis by assessment of digital reactive hyperemia. *J. Am. Coll. Cardiol.* **44**, 2137–2141 (2004).
20. J. Minami, M. Todoroki, T. Ishimitsu, H. Yamamoto, S. Abe, T. Fukunaga, H. Matsuoka, Effects of alcohol intake on ambulatory blood pressure, heart rate, and heart rate variability in Japanese men with different ALDH2 genotypes. *J. Hum. Hypertens.* **16**, 345–351 (2002).
21. M. J. Shin, Y. Cho, G. Davey Smith, Alcohol consumption, aldehyde dehydrogenase 2 gene polymorphisms, and cardiovascular health in Korea. *Yonsei Med. J.* **58**, 689–696 (2017).
22. Y. C. Chen, G. S. Peng, T. P. Tsao, M. F. Wang, R. B. Lu, S. J. Yin, Pharmacokinetic and pharmacodynamic basis for overcoming acetaldehyde-induced adverse reaction in Asian alcoholics, heterozygous for the variant ALDH2*2 gene allele. *Pharmacogenet. Genomics* **19**, 588–599 (2009).
23. A. Xue, L. Jiang, Z. Zhu, N. R. Wray, P. M. Visscher, J. Zeng, J. Yang, Genome-wide analyses of behavioural traits are subject to bias by misreports and longitudinal changes. *Nat. Commun.* **12**, 20211 (2021).
24. A. D. Ebert, K. Kodo, P. Liang, H. Wu, B. C. Huber, J. Riegler, J. Churko, J. Lee, P. de Almeida, F. Lan, S. Diecke, P. W. Burridge, J. D. Gold, D. Mochly-Rosen, J. C. Wu, Characterization of the molecular mechanisms underlying increased ischemic damage in the aldehyde dehydrogenase 2 genetic polymorphism using a human induced pluripotent stem cell model system. *Sci. Transl. Med.* **6**, 255ra130 (2014).
25. M. Gu, Efficient differentiation of human pluripotent stem cells to endothelial cells. *Curr. Protoc. Hum. Genet.* , e64 (2018).
26. V. O. Zambelli, E. R. Gross, C. H. Chen, V. P. Gutierrez, Y. Cury, D. Mochly-Rosen, Aldehyde dehydrogenase-2 regulates nociception in rodent models of acute inflammatory pain. *Sci. Transl. Med.* **6**, 251ra118 (2014).
27. S. Jin, J. Chen, L. Chen, G. Histen, Z. Lin, S. Gross, J. Hixon, Y. Chen, C. Kung, Y. Chen, Y. Fu, Y. Lu, H. Lin, X. Cai, H. Yang, R. A. Cairns, M. Dorsch, S. M. Su, S. Biller, T. W. Mak, Y. Cang, ALDH2(E487K) mutation increases protein turnover and promotes murine hepatocarcinogenesis. *Proc. Natl. Acad. Sci. U.S.A.* **112**, 9088–9093 (2015).
28. C. H. Chen, J. C. Ferreira, E. R. Gross, D. Mochly-Rosen, Targeting aldehyde dehydrogenase 2: New therapeutic opportunities. *Physiol. Rev.* **94**, 1–34 (2014).
29. K. Kaur, G. Bedi, M. Kaur, A. Vij, I. Kaur, Lipid peroxidation and the levels of antioxidant enzymes in coronary artery disease. *Indian J. Clin. Biochem.* **23**, 33–37 (2008).
30. D. Tousoulis, A. M. Kampoli, C. Tentolouris, N. Papageorgiou, C. Stefanadis, The role of nitric oxide on endothelial function. *Curr. Vasc. Pharmacol.* **10**, 4–18 (2012).
31. V. M. Victor, M. Rocha, E. Sola, C. Banuls, K. Garcia-Malpartida, A. Hernandez-Mijares, Oxidative stress, endothelial dysfunction and atherosclerosis. *Curr. Pharm. Des.* **15**, 2988–3002 (2009).
32. P. A. Cahill, E. M. Redmond, Alcohol and cardiovascular disease—Modulation of vascular cell function. *Nutrients* **4**, 297–318 (2012).
33. C. G. Kevil, R. P. Patel, D. C. Bullard, Essential role of ICAM-1 in mediating monocyte adhesion to aortic endothelial cells. *Am. J. Physiol. Cell Physiol.* **281**, C1442–C1447 (2001).
34. B. J. Jefferis, O. Papacosta, C. G. Owen, S. G. Wannamethee, S. E. Humphries, M. Woodward, L. T. Lennon, A. Thomson, P. Welsh, A. Rumley, G. D. Lowe, P. H. Whincup, Interleukin 18 and coronary heart disease: Prospective study and systematic review. *Atherosclerosis* **217**, 227–233 (2011).
35. D. J. Conklin, P. Haberzettl, R. A. Prough, A. Bhatnagar, Glutathione-S-transferase P protects against endothelial dysfunction induced by exposure to tobacco smoke. *Am. J. Physiol. Heart Circ. Physiol.* **296**, H1586–H1597 (2009).
36. A. Phulukdaree, S. Khan, D. Moodley, A. A. Chuturgoon, GST polymorphisms and early-onset coronary artery disease in young South African Indians. *S. Afr. Med. J.* **102**, 627–630 (2012).
37. P. Dufourcq, L. Leroux, J. Ezan, B. Descamps, J. M. Lamaziere, P. Costet, C. Basoni, C. Moreau, U. Deutsch, T. Couffinhal, C. Duplaa, Regulation of endothelial cell cytoskeletal reorganization by a secreted frizzled-related protein-1 and frizzled 4- and frizzled 7-dependent pathway: Role in neovessel formation. *Am. J. Pathol.* **172**, 37–49 (2008).
38. I. Shiojima, K. Walsh, Role of Akt signaling in vascular homeostasis and angiogenesis. *Circ. Res.* **90**, 1243–1250 (2002).
39. S. Dimmeler, I. Fleming, B. Fisslthaler, C. Hermann, R. Busse, A. M. Zeiher, Activation of nitric oxide synthase in endothelial cells by Akt-dependent phosphorylation. *Nature* **399**, 601–605 (1999).
40. G. M. Nitulescu, M. Van De Venter, G. Nitulescu, A. Ungurianu, P. Juzenas, Q. Peng, O. T. Olaru, D. Gradinaru, A. Tsatsakis, D. Tsoukalas, D. A. Spandidos, D. Margina, The Akt pathway in oncology therapy and beyond (Review). *Int. J. Oncol.* **53**, 2319–2331 (2018).
41. D. T. Paik, M. Chandy, J. C. Wu, Patient and disease-specific induced pluripotent stem cells for discovery of personalized cardiovascular drugs and therapeutics. *Pharmacol. Rev.* **72**, 320–342 (2020).
42. G. D. Lopaschuk, S. Verma, Mechanisms of cardiovascular benefits of sodium glucose co-transporter 2 (SGLT2) inhibitors: A state-of-the-art review. *JACC Basic Transl. Sci.* **5**, 632–644 (2020).
43. L. Uthman, A. Homayr, R. P. Juni, E. L. Spin, R. Kerindongo, M. Boomsma, M. W. Hollmann, B. Preckel, P. Koolwijk, V. W. M. van Hinsbergh, C. J. Zuurbier, M. Albrecht, N. C. Weber, Empagliflozin and dapagliflozin reduce ROS generation and restore NO bioavailability in tumor necrosis factor α-stimulated human coronary arterial endothelial cells. *Cell. Physiol. Biochem.* **53**, 865–886 (2019).
44. C. H. Chen, G. R. Budas, E. N. Churchill, M. H. Disatnik, T. D. Hurley, D. Mochly-Rosen, Activation of aldehyde dehydrogenase-2 reduces ischemic damage to the heart. *Science* **321**, 1493–1495 (2008).
45. R. Kudo, K. Yuui, S. Kasuda, K. Hatake, Effect of alcohol on vascular function. *Nihon Arukoru Yakubutsu Igakkai Zasshi* **50**, 123–134 (2015).
46. G. Pan, B. Roy, S. S. Palaniyandi, Diabetic aldehyde dehydrogenase 2 mutant (ALDH2*2) mice are more susceptible to cardiac ischemic-reperfusion injury due to 4-hydroxy-2-nonenal induced coronary endothelial cell damage. *J. Am. Heart Assoc.* **10**, e021140 (2021).
47. G. Pan, M. Deshpande, H. Pang, S. S. Palaniyandi, Precision medicine approach: Empagliflozin for diabetic cardiomyopathy in mice with aldehyde dehydrogenase (ALDH) 2*2 mutation, a specific genetic mutation in millions of East Asians. *Eur. J. Pharmacol.* **839**, 76–81 (2018).
48. S. Perez-Miller, H. Younus, R. Vanam, C. H. Chen, D. Mochly-Rosen, T. D. Hurley, Alda-1 is an agonist and chemical chaperone for the common human aldehyde dehydrogenase 2 variant. *Nat. Struct. Mol. Biol.* **17**, 159–164 (2010).
49. L. Uthman, A. Baartscheer, C. A. Schumacher, J. W. T. Fiolet, M. C. Kuschma, M. W. Hollmann, R. Coronel, N. C. Weber, C. J. Zuurbier, Direct cardiac actions of sodium glucose cotransporter 2 inhibitors target pathogenic mechanisms underlying heart failure in diabetic patients. *Front. Physiol.* **9**, 1575 (2018).
50. S. Chen, R. Coronel, M. W. Hollmann, N. C. Weber, C. J. Zuurbier, Direct cardiac effects of SGLT2 inhibitors. *Cardiovasc. Diabetol.* **21**, 45 (2022).
51. L. Uthman, X. Li, A. Baartscheer, C. A. Schumacher, P. Baumgart, J. Hermanides, B. Preckel, M. W. Hollmann, R. Coronel, C. J. Zuurbier, N. C. Weber, Empagliflozin reduces oxidative stress through inhibition of the novel inflammation/NHE/[$Na^+$]c/ROS-pathway in human endothelial cells. *Biomed. Pharmacother.* **146**, 112515 (2022).
52. Y. Dong, Y. Gao, A. Ilie, D. Kim, A. Boucher, B. Li, X. C. Zhang, J. Orlowski, Y. Zhao, Structure and mechanism of the human NHE1-CHP1 complex. *Nat. Commun.* **12**, 3474 (2021).
53. X. Li, B. Preckel, J. Hermanides, M. W. Hollmann, C. J. Zuurbier, N. C. Weber, Amelioration of endothelial dysfunction by sodium glucose co-transporter 2 inhibitors: Pieces of the puzzle explaining their cardiovascular protection. *Br. J. Pharmacol.* **179**, 4047–4062 (2022).
54. C. H. Chen, B. R. Kraemer, D. Mochly-Rosen, ALDH2 variance in disease and populations. *Dis. Model. Mech.* **15**, (2022).
55. P. Rajendran, T. Rengarajan, J. Thangavel, Y. Nishigaki, D. Sakthisekaran, G. Sethi, I. Nishigaki, The vascular endothelium and human diseases. *Int. J. Biol. Sci.* **9**, 1057–1069 (2013).
56. Y. Mizuno, S. Hokimoto, E. Harada, K. Kinoshita, K. Nakagawa, M. Yoshimura, H. Ogawa, H. Yasue, Variant aldehyde dehydrogenase 2 (ALDH2*2) is a risk factor for coronary spasm and ST-segment elevation myocardial infarction. *J. Am. Heart Assoc.* **5**, (2016).
57. P. Y. Chia, A. Teo, T. W. Yeo, Overview of the assessment of endothelial function in humans. *Front. Med.* **7**, 542567 (2020).
58. A. Yokoyama, H. Kato, T. Yokoyama, T. Tsujinaka, M. Muto, T. Omori, T. Haneda, Y. Kumagai, H. Igaki, M. Yokoyama, H. Watanabe, H. Fukuda, H. Yoshimizu, Genetic polymorphisms of alcohol and aldehyde dehydrogenases and glutathione S-transferase M1 and drinking, smoking, and diet in Japanese men with esophageal squamous cell carcinoma. *Carcinogenesis* **23**, 1851–1859 (2002).

59. S. Higuchi, S. Matsushita, H. Imazeki, T. Kinoshita, S. Takagi, H. Kono, Aldehyde dehydrogenase genotypes in Japanese alcoholics. *Lancet* **343**, 741–742 (1994).
60. H. Ma, R. Guo, L. Yu, Y. Zhang, J. Ren, Aldehyde dehydrogenase 2 (ALDH2) rescues myocardial ischaemia/reperfusion injury: Role of autophagy paradox and toxic aldehyde. *Eur. Heart J.* **32**, 1025–1038 (2011).
61. B. Perry, J. Banyard, E. R. McLaughlin, R. Watnick, A. Sohn, D. N. Brindley, T. Obata, L. C. Cantley, C. Cohen, J. L. Arbiser, AKT1 overexpression in endothelial cells leads to the development of cutaneous vascular malformations in vivo. *Arch. Dermatol.* **143**, 504–506 (2007).
62. S. Ghosh Dastidar, J. B. Warner, D. R. Warner, C. J. McClain, I. A. Kirpich, Rodent models of alcoholic liver disease: Role of binge ethanol administration. *Biomolecules* **8**, 3 (2018).
63. A. U. Joshi, L. D. Van Wassenhove, K. R. Logas, P. S. Minhas, K. I. Andreasson, K. I. Weinberg, C. H. Chen, D. Mochly-Rosen, Aldehyde dehydrogenase 2 activity and aldehydic load contribute to neuroinflammation and Alzheimer's disease related pathology. *Acta Neuropathol. Commun.* **7**, 190 (2019).
64. S. Zhong, L. Li, Y. L. Zhang, L. Zhang, J. Lu, S. Guo, N. Liang, J. Ge, M. Zhu, Y. Tao, Y. C. Wu, H. Yin, Acetaldehyde dehydrogenase 2 interactions with LDLR and AMPK regulate foam cell formation. *J. Clin. Invest.* **129**, 252–267 (2019).
65. G. Pan, B. Roy, S. Giri, D. E. Lanfear, R. A. Thandavarayan, A. Guha, P. A. Ortiz, S. S. Palaniyandi, Aldehyde dehydrogenase 2 activator augments the beneficial effects of empagliflozin in mice with diabetes-associated HFpEF. *Int. J. Mol. Sci.* **23**, (2022).
66. G. Palmiero, A. Cesaro, E. Vetrano, P. C. Pafundi, R. Galiero, A. Caturano, E. Moscarella, F. Gragnano, T. Salvatore, L. Rinaldi, P. Calabro, F. C. Sasso, Impact of SGLT2 inhibitors on heart failure: From pathophysiology to clinical effects. *Int. J. Mol. Sci.* **22**, (2021).
67. S. Steven, M. Oelze, A. Hanf, S. Kroller-Schon, F. Kashani, S. Roohani, P. Welschof, M. Kopp, U. Godtel-Armbrust, N. Xia, H. Li, E. Schulz, K. J. Lackner, L. Wojnowski, S. P. Bottari, P. Wenzel, E. Mayoux, T. Munzel, A. Daiber, The SGLT2 inhibitor empagliflozin improves the primary diabetic complications in ZDF rats. *Redox Biol.* **13**, 370–385 (2017).
68. O. Iborra-Egea, E. Santiago-Vacas, S. R. Yurista, J. Lupon, M. Packer, S. Heymans, F. Zannad, J. Butler, D. Pascual-Figal, A. Lax, J. Nunez, R. A. de Boer, A. Bayes-Genis, Unraveling the molecular mechanism of action of empagliflozin in heart failure with reduced ejection fraction with or without diabetes. *JACC Basic Transl. Sci.* **4**, 831–840 (2019).
69. H. Zhou, S. Wang, P. Zhu, S. Hu, Y. Chen, J. Ren, Empagliflozin rescues diabetic myocardial microvascular injury via AMPK-mediated inhibition of mitochondrial fission. *Redox Biol.* **15**, 335–346 (2018).
70. M. Nakao, I. Shimizu, G. Katsuumi, Y. Yoshida, M. Suda, Y. Hayashi, R. Ikegami, Y. T. Hsiao, S. Okuda, T. Soga, T. Minamino, Empagliflozin maintains capillarization and improves cardiac function in a murine model of left ventricular pressure overload. *Sci. Rep.* **11**, 18384 (2021).
71. L. Uthman, R. Nederlof, O. Eerbeek, A. Baartscheer, C. Schumacher, N. Buchholtz, M. W. Hollmann, R. Coronel, N. C. Weber, C. J. Zuurbier, Delayed ischaemic contracture onset by empagliflozin associates with NHE1 inhibition and is dependent on insulin in isolated mouse hearts. *Cardiovasc. Res.* **115**, 1533–1545 (2019).
72. A. Baartscheer, C. A. Schumacher, R. C. Wust, J. W. Fiolet, G. J. Stienen, R. Coronel, C. J. Zuurbier, Empagliflozin decreases myocardial cytoplasmic $Na^+$ through inhibition of the cardiac $Na^+/H^+$ exchanger in rats and rabbits. *Diabetologia* **60**, 568–573 (2017).
73. M. Trum, J. Riechel, S. Lebek, S. Pabel, S. T. Sossalla, S. Hirt, M. Arzt, L. S. Maier, S. Wagner, Empagliflozin inhibits $Na^+$ /$H^+$ exchanger activity in human atrial cardiomyocytes. *ESC Heart Fail.* **7**, 4429–4437 (2020).
74. C. J. Zuurbier, A. Baartscheer, C. A. Schumacher, J. W. T. Fiolet, R. Coronel, Sodium-glucose co-transporter 2 inhibitor empagliflozin inhibits the cardiac Na+/H+ exchanger 1: Persistent inhibition under various experimental conditions. *Cardiovasc. Res.* **117**, 2699–2701 (2021).
75. P. Theroux, B. R. Chaitman, N. Danchin, L. Erhardt, T. Meinertz, J. S. Schroeder, G. Tognoni, H. D. White, J. T. Willerson, A. Jessel, Inhibition of the sodium-hydrogen exchanger with cariporide to prevent myocardial infarction in high-risk ischemic situations. Main results of the GUARDIAN trial. Guard during ischemia against necrosis (GUARDIAN) Investigators. *Circulation* **102**, 3032–3038 (2000).
76. Y. Lin, C. Luo, Y. Shi, R. Ma, Q. Xia, W. Ding, The role of cariporide in protecting saphenous vein among different aldehyde dehydrogenase genotypes. *Cardiology* **145**, 456–466 (2020).
77. G. Nannelli, M. Ziche, S. Donnini, L. Morbidelli, Endothelial aldehyde dehydrogenase 2 as a target to maintain vascular wellness and function in ageing. *Biomedicine* **8**, (2020).
78. K. Ishigaki, M. Akiyama, M. Kanai, A. Takahashi, E. Kawakami, H. Sugishita, S. Sakaue, N. Matoba, S. K. Low, Y. Okada, C. Terao, T. Amariuta, S. Gazal, Y. Kochi, M. Horikoshi, K. Suzuki, K. Ito, S. Koyama, K. Ozaki, S. Niida, Y. Sakata, Y. Sakata, T. Kohno, K. Shiraishi, Y. Momozawa, M. Hirata, K. Matsuda, M. Ikeda, N. Iwata, S. Ikegawa, I. Kou, T. Tanaka, H. Nakagawa, A. Suzuki, T. Hirota, M. Tamari, K. Chayama, D. Miki, M. Mori, S. Nagayama, Y. Daigo, Y. Miki, T. Katagiri, O. Ogawa, W. Obara, H. Ito, T. Yoshida, I. Imoto, T. Takahashi, C. Tanikawa, T. Suzuki, N. Sinozaki, S. Minami, H. Yamaguchi, S. Asai, Y. Takahashi, K. Yamaji, K. Takahashi, T. Fujioka, R. Takata, H. Yanai, A. Masumoto, Y. Koretsune, H. Kutsumi, M. Higashiyama, S. Murayama, N. Minegishi, K. Suzuki, K. Tanno, A. Shimizu, T. Yamaji, M. Iwasaki, N. Sawada, H. Uemura, K. Tanaka, M. Naito, M. Sasaki, K. Wakai, S. Tsugane, M. Yamamoto, K. Yamamoto, Y. Murakami, Y. Nakamura, S. Raychaudhuri, J. Inazawa, T. Yamauchi, T. Kadowaki, M. Kubo, Y. Kamatani, Large-scale genome-wide association study in a Japanese population identifies novel susceptibility loci across different dise1ases. *Nat. Genet.* **52**, 669–679 (2020).
79. R. J. Pruim, R. P. Welch, S. Sanna, T. M. Teslovich, P. S. Chines, T. P. Gliedt, M. Boehnke, G. R. Abecasis, C. J. Willer, LocusZoom: Regional visualization of genome-wide association scan results. *Bioinformatics* **26**, 2336–2337 (2010).
80. N. Sayed, C. Liu, M. Ameen, F. Himmati, J. Z. Zhang, S. Khanamiri, J. R. Moonen, A. Wnorowski, L. Cheng, J. W. Rhee, S. Gaddam, K. C. Wang, K. Sallam, J. H. Boyd, Y. J. Woo, M. Rabinovitch, J. C. Wu, Clinical trial in a dish using iPSCs shows lovastatin improves endothelial dysfunction and cellular cross-talk in LMNA cardiomyopathy. *Sci. Transl. Med.* **12**, (2020).
81. X. Wang, C. Zeng, H. Gong, H. He, M. Wang, Q. Hu, F. Yang, The influence of nitroglycerin on the proliferation of endothelial progenitor cells from peripheral blood of patients with coronary artery disease. *Acta Biochim. Biophys. Sin.* **46**, 851–858 (2014).
82. G. Carpentier, S. Berndt, S. Ferratge, W. Rasband, M. Cuendet, G. Uzan, P. Albanese, Angiogenesis analyzer for ImageJ—A comparative morphometric analysis of "endothelial tube formation assay" and "fibrin bead assay". *Sci. Rep.* **10**, 11568 (2020).
83. M. Jamal, K. Ameno, N. Tanaka, A. Ito, A. Takakura, M. Kumihashi, H. Kinoshita, Ethanol and acetaldehyde after intraperitoneal administration to Aldh2-knockout mice-reflection in blood and brain levels. *Neurochem. Res.* **41**, 1029–1034 (2016).
84. B. L. Furman, Streptozotocin-induced diabetic models in mice and rats. *Curr. Protoc. Pharmacol.* **70**, 5.47.1–5.47.20 (2015).
85. E. Braun, J. Gilmer, H. B. Mayes, D. L. Mobley, J. I. Monroe, S. Prasad, D. M. Zuckerman, Best practices for foundations in molecular simulations [article v1.0]. *Living J. Comput. Mol. Sci.* **1**, 5957 (2019).
86. K. H. Lee, H. S. Kim, H. S. Jeong, Y. S. Lee, Chaperonin GroESL mediates the protein folding of human liver mitochondrial aldehyde dehydrogenase in Escherichia coli. *Biochem. Biophys. Res. Commun.* **298**, 216–224 (2002).
87. C. H. Chen, J. C. B. Ferreira, A. U. Joshi, M. C. Stevens, S. J. Li, J. H. Hsu, R. Maclean, N. D. Ferreira, P. R. Cervantes, D. D. Martinez, F. L. Barrientos, G. H. R. Quintanares, D. Mochly-Rosen, Novel and prevalent non-East Asian ALDH2 variants; implications for global susceptibility to aldehydes' toxicity. *EBioMedicine* **55**, 102753 (2020).
88. J. Z. Zhang, S. R. Zhao, C. Tu, P. Pang, M. Zhang, J. C. Wu, Protocol to measure contraction, calcium, and action potential in human-induced pluripotent stem cell-derived cardiomyocytes. *STAR Protoc.* **2**, 100859 (2021).


**Acknowledgments:** We thank N. Leeper and H. Zhu for assistance with the EndoPAT experimentation and analysis. We also thank all the recruited human participants for participating in this study. We thank B. Wu and M. Nishiga for helpful editing on the manuscript. We also thank G. Pan at Henry Ford Health System for advice on establishing STZ-induced diabetic mice. **Funding:** This work was supported by NIH grants K99 HL150319 (to H.G.), K99 HL150216 (to D.T.P.), R01 AA11147 (to D.M.-R.), R35 GM119522 (to E.R.G.), R01 HL130020 (to J.C.W.), R01 HL126527 (to J.C.W.), R01 HL113006 (to J.C.W.), R01 HL146690 (to J.C.W.), and P01 HL141084 (to J.C.W.); American Heart Association grant 20CDA35260261 (to D.T.P.); and Tobacco-Related Disease Research Program T31FT1392 (to X.Y.). **Author contributions:** Study design: H.G. and J.C.W. EndoPAT assessment: H.G. and A.M. Animal experiments: H.G. and X.Y. Biobank Japan analysis: J.M.J. and Y.L. In silico analysis: R.S., S.M., A.Z., and S.P. Cell differentiation and functional assays: H.G., D.T.P., J.W.J., T.Z., and W.W. Biochemical assays: F.R. and D.J.S. RNA-seq analysis: Y.L. Electrophysiological studies: S.R.Z. Writing, reviewing, and editing: H.G., X.Y., Y.L., M.C., D.T.P., J.C.W., M.A.R., E.R.G., D.M.-R., and C.-H.C. **Competing interests:** D.M.-R. and C.-H.C. hold patents related to Alda-1 activation of ALDH2. One of the patents is licensed to Foresee Pharmaceuticals, a company at which D.M.-R. is a consultant. J.C.W. is a cofounder of Greenstone Biosciences. M.C. is a consultant for Greenstone Biosciences. **Data and materials availability:** All data associated with this study are present in the paper or the Supplementary Materials. RNA-seq data generated for this study are deposited at the Gene Expression Omnibus in the NCBI database under the accession number GSE184419. All code is available at https://zenodo.org/record/7478648.

Submitted 11 March 2022
Accepted 4 January 2023
Published 25 January 2023
10.1126/scitranslmed.abp9952